Robotica (2022), **40**, pp. 646–671
doi:10.1017/S0263574721000746

CAMBRIDGE UNIVERSITY PRESS

RESEARCH ARTICLE

Dynamic modeling and power optimization of a 4RPSP+PS parallel flight simulator machine

Soheil Zarkandi*

Department of Mechanical Engineering, Babol Noshirvani University of Technology, Babol, Iran
*Corresponding author. Email: zarkandi@gmail.com

Received: 23 December 2020; **Revised:** 13 May 2021; **Accepted:** 13 May 2021; **First published online:** 16 June 2021

Keywords: flight simulator, parallel manipulator, 4 DOFs, dynamics, Euler–Lagrange method, SimMechanics, power optimization, golden eagle optimizer

Abstract

Reducing consumed power of a robotic machine has an essential role in enhancing its energy efficiency and must be considered during its design process. This paper deals with dynamic modeling and power optimization of a four-degrees-of-freedom flight simulator machine. Simulator cabin of the machine has yaw, pitch, roll and heave motions produced by a 4RPSP+PS parallel manipulator (PM). Using the Euler–Lagrange method, a closed-form dynamic equation is derived for the 4RPSP+PS PM, and its power consumption is computed on the entire workspace. Then, a newly introduced optimization algorithm called multiobjective golden eagle optimizer is utilized to establish a Pareto front of optimal designs of the manipulator having a relatively larger workspace and lower power consumption. The results are verified through numerical examples.

1. Introduction

Flight simulators are machines for artificially creating flight of an aircraft and are used for a variety of reasons, including flight training, design and development of the aircraft itself, research into aircraft characteristics and control handling qualities [1]. The first parallel manipulator (PM) having six degrees-of-freedom (DOF) was introduced by Stewart [2] as a flight simulator. Since then PMs have been vastly employed in industry. For several specific tasks, PMs with less than six DOFs are more preferred, because they have simpler architecture, lower cost of manufacturing and larger workspace, compared to PMs with six DOFs, see, for instance [3, 4, 5, 6, 7, 8].

Dynamic modeling of PMs is utilized in computer simulation for finding their dynamic characteristics, [4, 5, 6, 7, 9, 10] and also used for the development of suitable control strategies of PMs [11, 12]. Moreover, it specifies all joint forces and moments that are necessary for sizing links, bearings and actuators [13]. The dynamic analysis of PMs is divided into two branches [14]: the inverse dynamic analysis which computes the required actuator forces or torques necessary to generate a desired trajectory of the moving platform, and the forward dynamic analysis which finds resulting motion of the moving platform for a given forces or torques applied to actuators. The inverse dynamic analysis is often used for real-time feed-forward control of a manipulator, while the forward dynamic analysis is primarily applied to simulations of a manipulator. Several approaches have been employed for dynamic modeling of PMs. The main approaches are Newton–Euler method, [7, 15] Euler–Lagrange method [16, 17] and the principle of virtual work [18]. The Newton–Euler method formulates dynamic equations of motion for all moving links of the PM using the Newtonian mechanics. The Euler–Lagrange method is based on the kinetic and potential energies of the manipulator system and formulates dynamic equations of motion using Lagrangian functions. The principle of virtual work develops dynamic equations of motion using D'Alembert's principle stating that the work performed by external forces or moments through virtual

© The Author(s), 2021. Published by Cambridge University Press.

https://doi.org/10.1017/S0263574721000746 Published online by Cambridge University Press

displacements compatible with the system is zero. Other methods were also used by scholars for dynamic analysis of PMs, for instance, Kane's method, [19] combination of screw theory with the principle of virtual work, [20] natural orthogonal complement [21] and motor algebra [22]. Efficiency of the chosen method for dynamic analysis of a PM depends on DOF of the PM, complexity of the structure of the PM and so on.

In mechanical engineering, power consumption refers generally to the energy per unit time, supplied by actuators for a machine to accomplish a given task. The less the power consumption of a machine, the high its energy efficiency. The importance of this concept is testified by abundant literature including both theoretical and experimental studies for enhancing the energy efficiency in manipulators and automatic machines [23]. The main approaches to achieve this goal are: (1) the proper choice of the manipulator type, [24] (2) designing lightweight manipulators with lower inertia, [25, 26] (3) optimization of manipulator structure, [27] using regenerative drive systems, [28, 29] trajectory planning and motion planning, [30, 31, 32] applying redundancy on non-redundant manipulators, [33, 34, 35, 36] optimizing location of the task with respect to the base of the manipulator [37, 38] and joint force/torque minimization [13, 39, 40] and introduction of complaint or elastic elements into the manipulator [41, 42].

The above methods to evaluate power consumption of manipulators have some drawbacks. For instance, they are generally time-dependent and not suitable for instantaneous energy change evaluation. Moreover, they rely on the predefined trajectory and velocity of the end-effector, which are unchanged during the experiments. On the other hand, in most of the existing researches, the results are obtained regardless of the inherited relationship between energy consumption of the manipulator and its design variables, such as geometry, mass and inertia. To alleviate these drawbacks, Liu et al. [43] proposed a method to evaluate energy efficiency of parallel robot based on the kinetic energy change rate. Their method is a quantitative evaluation method rather than an experiment-based method. Besides, it is not focusing on specific trajectories or motions. The method builds the relationship between design parameters and energy efficiency of manipulators.

Recently, the author [44] introduced a 4-DOF PM with symmetrical 4RPSP+PS topology and studied its kinematics and workspace in detail. The letters R, P and S are representatives of a revolute joint, a prismatic joint and a spherical joint, respectively, and P denotes an actuated prismatic joint. A CAD model of the 4RPSP+PS PM is shown in Fig. 1. The moving platform of the manipulator is connected to the fixed platform (or the base) through one passive PS leg and four active RPSP legs. The PS leg is mounted at the center of the base platform, and RPSP legs are arranged symmetrically around it. Each RPSP leg has three links, a cylinder, a piston and a small block that are connected to each other and also to the fixed and moving platforms through R, P, S and P joints, respectively. The R joint is located on the plane of the fixed platform. The actuated P joint (or prismatic actuator) connects the cylinder to the piston. The S joint of RPSP leg is mounted on the small block sliding on the lower surface of the moving platform through a passive P joint.

The passive PS leg of the 4RPSP+PS PM constrains the moving platform to move along the vertical axis of its passive P joint, and simultaneously to rotate around the center of its S joint [44]. Thus, the moving platform has three rotational (yaw, pitch, roll) and one translational (heave) DOF. These special DOFs make the manipulator much more suitable for flight simulator machines, while simulator cabin of the machine is mounted on the moving platform (Fig. 1). Nevertheless, heavy weight of the simulator cabin increases power consumption of the manipulator during motion significantly. Therefore, a solution should be thought of to minimize power consumption of the manipulator. The main purpose of this paper is dynamic modeling and power optimization of the above 4RPSP+PS PM on its whole workspace, regardless of trajectories or motions of the moving platform.

The reminder of this paper is organized as follows. Some brief descriptions of the manipulator structure and its inverse position kinematics are presented in Sections 2 and 3. Jacobian matrices of the manipulator moving links are obtained in Section 4. Afterwards, in Section 5, through a complete dynamic modeling, a closed-form dynamic equation is derived for the manipulator. A global power

https://doi.org/10.1017/S0263574721000746 Published online by Cambridge University Press

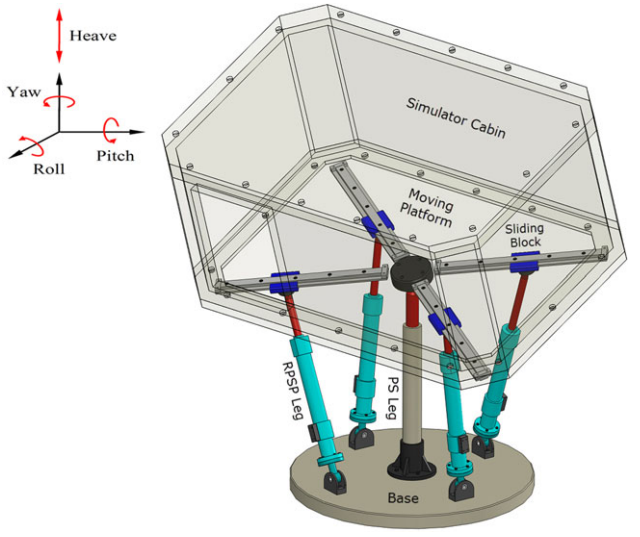

Figure 1. *A CAD model of the 4RPSP+PS flight simulator machine.*

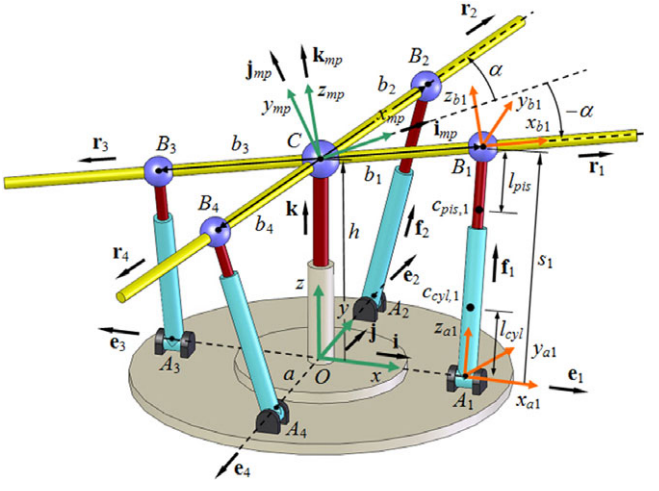

Figure 2. *Kinematic model of 4RPSP+PS PM.*

transmission index is defined in Section 6, and then applied in Section 7 for power optimization of the manipulator. Finally, a conclusion is given in Section 8 summarizing the present work.

2. Structure description of the 4RPSP+PS PM

Kinematic model of the symmetrical 4RPSP+PS PM is shown in Fig. 2. In this paper, subscript i refers to the ith RPSP leg of the manipulator for i = 1, 2, 3 and 4. Subscript mp refers to the moving platform, and subscripts cyl, pis and bl refer to the cylinder, piston and sliding block of the RPSP legs, respectively. Moreover, subscript pl refers to the passive PS leg. R (S) joint of the ith RPSP leg is located at Point A_i (B_i). Axes of R joints (passive P joints) of RPSP legs intersect at the centered point O (C). Axes of R joints are perpendicular to each other consecutively. Stroke of the actuated P joint (passive P joint) of the ith RPSP leg, shown by s_i (b_i), is the distance from point A_i (C) to point B_i. Axis of P joint of the PS leg is perpendicular to the plane of fixed platform, and its S joint is mounted

https://doi.org/10.1017/S0263574721000746 Published online by Cambridge University Press

at the center of the moving platform. Stroke of P joint of the PS leg, shown by h, is equal to the distance from point O to point C. A fixed coordinate frame O-xyz is attached at point O of the base plane while its x and y axes are coincident with the axes of the first and the second R joint, respectively. Thus, the z axis is along the axis of P joint of the PS leg. Another coordinate frame C-$x_{mp}y_{mp}z_{mp}$ is attached at point C of the moving platform plane, whereas x_{mp} (y_{mp}) axis locates on the interior bisector of the angle between the axes of passive P joints of the first (the second) and the second (the third) RPSP leg. The passive P joints of the RPSP legs are co-axis two by two. The angle between the x_{mp} axis and the axis of passive P joint of the first (the second) RPSP leg is shown by $-\alpha$ (α). Three unit vectors $\mathbf{i}$, $\mathbf{j}$ and $\mathbf{k}$ ($\mathbf{i}_{mp}$, $\mathbf{j}_{mp}$ and $\mathbf{k}_{mp}$) are considered along the x, y and z axes (x_{mp}, y_{mp} and z_{mp} axes), respectively. Unit vectors $\mathbf{e}_i$, $\mathbf{f}_i$ and $\mathbf{r}_i$ represent axes of R, P and P joint of the ith RPSP leg, respectively.

3. Inverse position kinematics

Pose of the moving platform is defined by pose vector $\mathbf{q} = [h\ \varphi_x\ \varphi_y\ \varphi_z]^T$ where Euler angles φ_x, φ_y and φ_z represent three successive rotations around the fixed x, y and z axes, respectively.

In ref. [44], it is shown that the inverse position kinematics of 4RPSP+PS PM, that is, determining actuator strokes s_i for the given pose vector $\mathbf{q}$ of the moving platform, leads to

$$s_i = \sqrt{(h\mathbf{k} + b_i\mathbf{R}_{mp}\mathbf{r}_{mp,i} - a\mathbf{e}_i)^T(h\mathbf{k} + b_i\mathbf{R}_{mp}\mathbf{r}_{mp,i} - a\mathbf{e}_i)} \tag{1}$$

where $\mathbf{r}_{mp,i}$ denotes vector $\mathbf{r}_i$ in the moving coordinate frame C-$x_{mp}y_{mp}z_{mp}$, such that

$$\mathbf{r}_{mp,1} = [\cos\alpha \quad -\sin\alpha \quad 0]^T \tag{2a}$$

$$\mathbf{r}_{mp,2} = [\cos\alpha \quad \sin\alpha \quad 0]^T \tag{2b}$$

$$\mathbf{r}_{mp,3} = -\mathbf{r}_{mp,1} \tag{2c}$$

$$\mathbf{r}_{mp,4} = -\mathbf{r}_{mp,2} \tag{2d}$$

and

$$\mathbf{e}_1 = [1 \quad 0 \quad 0]^T, \mathbf{e}_2 = [0\ 1\ 0]^T, \mathbf{e}_3 = -\mathbf{e}_1, \mathbf{e}_4 = -\mathbf{e}_2 \tag{3}$$

Moreover, $\mathbf{R}_{mp}$ is the rotation matrix of the frame C-$x_{mp}y_{mp}z_{mp}$ with respect to the base frame O-xyz, as follows:

$$\mathbf{R}_{mp} = \begin{bmatrix} c\varphi_z c\varphi_y & c\varphi_z s\varphi_y s\varphi_x - s\varphi_z c\varphi_x & c\varphi_z s\varphi_y c\varphi_x + s\varphi_z s\varphi_x \\ s\varphi_z c\varphi_y & s\varphi_z s\varphi_y s\varphi_x + c\varphi_z c\varphi_x & s\varphi_z s\varphi_y c\varphi_x - c\varphi_z s\varphi_x \\ -s\varphi_y & c\varphi_y s\varphi_x & c\varphi_y c\varphi_x \end{bmatrix} \tag{4}$$

where $s(.)$ and $c(.)$ denote sin(.) and cos(.), respectively, and three Euler angles φ_x, φ_y and φ_z are given as $\varphi_x \in (-\pi, \pi]$, $\varphi_y \in [-\pi/2, \pi/2]$ and $\varphi_z \in (-\pi, \pi]$. Consequently, direction of the ith RPSP leg will be obtained as [44]

$$\mathbf{f}_i = (h\mathbf{k} + b_i\mathbf{R}_{mp}\mathbf{r}_{mp,i} - a\mathbf{e}_i)/s_i \tag{5}$$

4. Jacobian matrices

4.1. Jacobian matrices of 4RPSP+PS PM

Let $\boldsymbol{\omega}_{mp} = [\dot{\varphi}_x\ \dot{\varphi}_y\ \dot{\varphi}_z]^T$ be angular velocity vector of the moving platform. The relation between velocity vector of the moving platform, $\dot{\mathbf{q}} = [\dot{h}\ \boldsymbol{\omega}_{mp}^T]^T$, and velocity vector of the actuated prismatic joints, $\dot{\mathbf{s}} = [\dot{s}_1\ \dot{s}_2\ \dot{s}_3\ \dot{s}_4]^T$, is [44]

https://doi.org/10.1017/S0263574721000746 Published online by Cambridge University Press

$$\mathbf{J}_{inv}\dot{\mathbf{s}} = \mathbf{J}_{fwd}\dot{\mathbf{q}} \tag{6}$$

where $\mathbf{J}_{inv}$ and $\mathbf{J}_{fwd}$ are the 4×4 inverse and forward Jacobian matrices of the manipulator, respectively, and expressed as

$$\mathbf{J}_{inv} = \begin{bmatrix} d_1 & 0 & 0 & 0 \\ 0 & d_2 & 0 & 0 \\ 0 & 0 & d_3 & 0 \\ 0 & 0 & 0 & d_4 \end{bmatrix}_{4\times4} \tag{7a}$$

$$\mathbf{J}_{fwd} = \begin{bmatrix} ((\mathbf{e}_1 \times \mathbf{f}_1) \times \mathbf{r}_1)_z & b_1(\mathbf{r}_1 \times ((\mathbf{e}_1 \times \mathbf{f}_1) \times \mathbf{r}_1))^T \\ ((\mathbf{e}_2 \times \mathbf{f}_2) \times \mathbf{r}_2)_z & b_2(\mathbf{r}_2 \times ((\mathbf{e}_2 \times \mathbf{f}_2) \times \mathbf{r}_2))^T \\ ((\mathbf{e}_3 \times \mathbf{f}_3) \times \mathbf{r}_3)_z & b_3(\mathbf{r}_3 \times ((\mathbf{e}_3 \times \mathbf{f}_3) \times \mathbf{r}_3))^T \\ ((\mathbf{e}_4 \times \mathbf{f}_4) \times \mathbf{r}_4)_z & b_4(\mathbf{r}_4 \times ((\mathbf{e}_4 \times \mathbf{f}_4) \times \mathbf{r}_4))^T \end{bmatrix}_{4\times4} \tag{7b}$$

with

$$d_i = ((\mathbf{e}_i \times \mathbf{f}_i) \times \mathbf{r}_i)^T \mathbf{f}_i \tag{8}$$

If $\mathbf{J}_{fwd}$ is invertible, Eq. (6) can be rewritten as

$$\dot{\mathbf{q}} = \mathbf{J}_{PM}\dot{\mathbf{s}} \tag{9}$$

where

$$\mathbf{J}_{PM} = \mathbf{J}_{fwd}^{-1}\mathbf{J}_{inv} \tag{10}$$

is defined as the 4×4 Jacobian matrix of the 4RPSP+PS PM.

4.2. Jacobian matrices of the moving platform and simulator cabin

The linear velocity $\dot{h}\mathbf{k}$ of the moving platform can be written in terms of $\dot{\mathbf{q}}$ as follows:

$$\dot{h}\mathbf{k} = \mathbf{J}_{hmp}\dot{\mathbf{q}} \tag{11}$$

where 3×4 matrix $\mathbf{J}_{hmp}$ is

$$\mathbf{J}_{hmp} = \begin{bmatrix} 1 & \mathbf{0}_{1\times3} \\ 0 & \mathbf{0}_{1\times3} \\ 0 & \mathbf{0}_{1\times3} \end{bmatrix} \tag{12}$$

and for the angular velocity $\boldsymbol{\omega}_{mp}$, we can write

$$\boldsymbol{\omega}_{mp} = \mathbf{J}_{\omega mp}\dot{\mathbf{q}} \tag{13}$$

where the 3×4 matrix $\mathbf{J}_{\omega mp}$ is

$$\mathbf{J}_{\omega mp} = \begin{bmatrix} 0 & 1 & 0 & 0 \\ 0 & 0 & 1 & 0 \\ 0 & 0 & 0 & 1 \end{bmatrix} \tag{14}$$

Angular velocity of the simulator cabin attached to the moving platform is equal to $\boldsymbol{\omega}_{mp}$, and linear velocity of its mass center, c_{sc}, is

$$\mathbf{v}_{sc} = \dot{h}\mathbf{k} + \boldsymbol{\omega}_{mp} \times \mathbf{d}_{sc} \tag{15}$$

where $\mathbf{d}_{sc} = [d_{sc,x}, d_{sc,y}, d_{sc,z}]^T$ is the position vector of mass center of the simulator cabin with respect to point C (Fig. 3). Substituting $\dot{h}\mathbf{k}$ and $\boldsymbol{\omega}_{mp}$ from Eqs. (11) and (13) into Eq. (15) and rearranging the resultant equation lead to

$$\mathbf{v}_{sc} = \mathbf{J}_{sc}\dot{\mathbf{q}} \tag{16}$$

https://doi.org/10.1017/S0263574721000746 Published online by Cambridge University Press

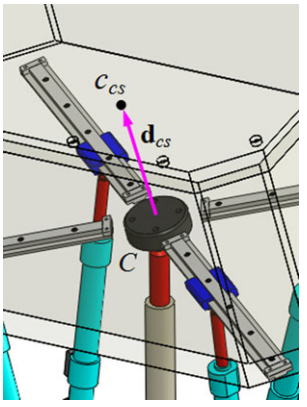

Figure 3. *Mass center c_{sc} of the simulator cabin.*

where 3×4 matrix $\mathbf{J}_{sc}$ is

$$\mathbf{J}_{sc} = \begin{bmatrix} 1 & 0 & d_{sc,z} & -d_{sc,y} \\ 0 & -d_{sc,z} & 0 & d_{sc,x} \\ 0 & d_{sc,y} & -d_{sc,x} & 0 \end{bmatrix} \tag{17}$$

4.3. Jacobian matrices of the RPSP legs

4.3.1. Jacobian matrices of cylinder and piston of the ith RPSP leg

The relation between velocities of the moving platform, PS leg and the *i*th RPSP leg is [44]

$$\dot{h}\mathbf{k} + \dot{b}_i\mathbf{r}_i + b_i\boldsymbol{\omega}_{mp} \times \mathbf{r}_i = \dot{s}_i\mathbf{f}_i + s_i\boldsymbol{\omega}_i \times \mathbf{f}_i \tag{18}$$

where $\dot{h}\mathbf{k}$ denotes linear velocity vector of the moving platform, and $\boldsymbol{\omega}_i$ is the angular velocity of the *i*th RPSP leg. Since the *i*th RPSP leg of the manipulator rotates about axis of the associate revolute joint at A_i, $\mathbf{v}_{Bi}$ has no component along $\mathbf{e}_i$, that is, $\mathbf{v}_{Bi}^T\mathbf{e}_i = 0$. The same is true for the velocity of point C, that is, $\dot{h}\mathbf{k}^T\mathbf{e}_i = 0$. Thus, dot multiplying both sides of Eq. (18) by $\mathbf{e}_i$ yields

$$\dot{b}_i\mathbf{r}_i^T\mathbf{e}_i + b_i(\boldsymbol{\omega}_{mp} \times \mathbf{r}_i)^T\mathbf{e}_i = 0 \tag{19}$$

from which we obtain

$$\dot{b}_i = -\frac{b_i(\boldsymbol{\omega}_{mp} \times \mathbf{r}_i)^T\mathbf{e}_i}{\mathbf{r}_i^T\mathbf{e}_i} \tag{20}$$

Cross multiplying both sides of Eq. (18) by $\mathbf{f}_i$ gives

$$\dot{h}\mathbf{k} \times \mathbf{f}_i + \dot{b}_i\mathbf{r}_i \times \mathbf{f}_i + b_i(\boldsymbol{\omega}_{mp} \times \mathbf{r}_i) \times \mathbf{f}_i = s_i(\boldsymbol{\omega}_i \times \mathbf{f}_i) \times \mathbf{f}_i \tag{21}$$

Since $\boldsymbol{\omega}_i$ is along $\mathbf{e}_i$, we have $(\boldsymbol{\omega}_i \times \mathbf{f}_i) \times \mathbf{f}_i = -\boldsymbol{\omega}_i$, and consequently Eq. (21) gives

$$\boldsymbol{\omega}_i = -(1/s_i)(\dot{h}\mathbf{k} \times \mathbf{f}_i + \dot{b}_i\mathbf{r}_i \times \mathbf{f}_i + b_i(\boldsymbol{\omega}_{mp} \times \mathbf{r}_i) \times \mathbf{f}_i) \tag{22}$$

Based on the linear algebra, the third term on the right-hand side of Eq. (22) can be rewritten as

$$(\boldsymbol{\omega}_{mp} \times \mathbf{r}_i) \times \mathbf{f}_i = (\boldsymbol{\omega}_{mp}^T\mathbf{f}_i) - (\boldsymbol{\omega}_{mp}^T\mathbf{r}_i)\mathbf{f}_i \tag{23}$$

Substituting Eqs. (11), (20), (13) and (23) into Eq. (22) results in

$$\boldsymbol{\omega}_i = -(1/s_i)(\mathbf{J}_{hmp}\dot{\mathbf{q}} \times \mathbf{f}_i - \frac{b_i(\mathbf{r}_i \times \mathbf{e}_i)\mathbf{J}_{\omega mp}\dot{\mathbf{q}}}{\mathbf{r}_i^T\mathbf{e}_i}\mathbf{r}_i \times \mathbf{f}_i - b_i((\mathbf{f}_i^T\mathbf{r}_i)\mathbf{J}_{\omega mp}\dot{\mathbf{q}} - (\mathbf{f}_i^T\mathbf{J}_{\omega mp}\dot{\mathbf{q}})\mathbf{r}_i) \tag{24}$$

Writing Eq. (24) in a matrix form gives $\boldsymbol{\omega}_i$ in terms of $\dot{\mathbf{q}}$ as follows:

$$\boldsymbol{\omega}_i = \mathbf{J}_{\omega i}\dot{\mathbf{q}} \tag{25}$$

https://doi.org/10.1017/S0263574721000746 Published online by Cambridge University Press

where the 3×4 matrix $\mathbf{J}_{\omega i}$ will be

$$\mathbf{J}_{\omega i} = \sum_{k=1}^{3} \mathbf{J}_{\omega i,k} \tag{26}$$

with

$$\mathbf{J}_{\omega i,1} = -(1/s_i) \begin{bmatrix} f_{iz}\mathbf{J}_{hmp,2\times(1-4)} - f_{iy}\mathbf{J}_{hmp,3\times(1-4)} \\ f_{ix}\mathbf{J}_{hmp,3\times(1-4)} - f_{iz}\mathbf{J}_{hmp,1\times(1-4)} \\ f_{iy}\mathbf{J}_{hmp,1\times(1-4)} - f_{ix}\mathbf{J}_{hmp,2\times(1-4)} \end{bmatrix} \tag{27a}$$

$$\mathbf{J}_{\omega i,2} = -(b_i/\mathbf{r}_i^T\mathbf{e}_i) \begin{bmatrix} (\mathbf{r}_i \times \mathbf{e}_i)^T\mathbf{J}_{\omega mp}(r_{iz}f_{iy} - r_{iy}f_{iz}) \\ (\mathbf{r}_i \times \mathbf{e}_i)^T\mathbf{J}_{\omega mp}(r_{ix}f_{iz} - r_{iz}f_{ix}) \\ (\mathbf{r}_i \times \mathbf{e}_i)^T\mathbf{J}_{\omega mp}(r_{iy}f_{ix} - r_{ix}f_{iy}) \end{bmatrix} \tag{27b}$$

$$\mathbf{J}_{\omega i,3} = -b_i((\mathbf{f}_i^T\mathbf{r}_i)\mathbf{J}_{\omega mp} + \begin{bmatrix} \mathbf{f}_i^T\mathbf{J}_{\omega mp}r_{ix} \\ \mathbf{f}_i^T\mathbf{J}_{\omega mp}r_{iy} \\ \mathbf{f}_i^T\mathbf{J}_{\omega mp}r_{iz} \end{bmatrix} \tag{27c}$$

With reference to Fig. 2, velocities of mass centers of cylinder and piston of the ith R$\underline{\text{P}}$SP leg are computed using the following relations, respectively:

$$\mathbf{v}_{cyl,i} = l_{cyl}\boldsymbol{\omega}_i \times \mathbf{f}_i \tag{28a}$$

$$\mathbf{v}_{pis,i} = (s_i - l_{pis})\boldsymbol{\omega}_i \times \mathbf{f}_i + \dot{s}_i\mathbf{f}_i \tag{28b}$$

From Eq. (9), variable $\dot{s}_i$ can be determined in terms of $\dot{\mathbf{q}}$ as

$$\dot{s}_i = \mathbf{J}_{PM,i\times(1-4)}^{-1}\dot{\mathbf{q}} \tag{29}$$

where $\mathbf{J}_{PM,i\times(1-4)}^{-1}$ denotes the ith row of the inverse matrix $\mathbf{J}_{PM}^{-1}$. Substituting $\boldsymbol{\omega}_i$ and $\dot{s}_i$ from Eqs. (25) and (29) into Eqs. (28) and doing some rearranging lead to

$$\mathbf{v}_{cyl,i} = \mathbf{J}_{cyl,i}\dot{\mathbf{q}} \tag{30a}$$

$$\mathbf{v}_{pis,i} = \mathbf{J}_{pis,i}\dot{\mathbf{q}} \tag{30b}$$

where the 3×4 matrices $\mathbf{J}_{cyl,i}$ and $\mathbf{J}_{pis,i}$ are defined as

$$\mathbf{J}_{cyl,i} = \begin{bmatrix} l_{cyl}(f_{iz}\mathbf{J}_{\omega i,2\times(1-4)} - f_{iy}\mathbf{J}_{\omega i,3\times(1-4)}) \\ l_{cyl}(f_{ix}\mathbf{J}_{\omega i,3\times(1-4)} - f_{iz}\mathbf{J}_{\omega i,1\times(1-4)}) \\ l_{cyl}(f_{iy}\mathbf{J}_{\omega i,1\times(1-4)} - f_{ix}\mathbf{J}_{\omega i,2\times(1-4)}) \end{bmatrix} \tag{31a}$$

$$\mathbf{J}_{pis,i} = \begin{bmatrix} (s_i - l_{pis})(f_{iz}\mathbf{J}_{\omega i,2\times(1-4)} - f_{iy}\mathbf{J}_{\omega i,3\times(1-4)}) + f_{ix}\mathbf{J}_{\omega i\times(1-4)}^{-1}\mathbf{J}_{mp} \\ (s_i - l_{pis})(f_{ix}\mathbf{J}_{\omega i,3\times(1-4)} - f_{iz}\mathbf{J}_{\omega i,1\times(1-4)}) + f_{iy}\mathbf{J}_{\omega i\times(1-4)}^{-1}\mathbf{J}_{mp} \\ (s_i - l_{pis})(f_{iy}\mathbf{J}_{\omega i,1\times(1-4)} - f_{ix}\mathbf{J}_{\omega i,2\times(1-4)}) + f_{iz}\mathbf{J}_{\omega i\times(1-4)}^{-1}\mathbf{J}_{mp} \end{bmatrix} \tag{31b}$$

4.3.2. Jacobian matrix of sliding block of the ith R$\underline{\text{P}}$SP leg

Sliding block of the ith R$\underline{\text{P}}$SP leg has no rotational motion with respect to the moving platform, so angular velocity of the ith sliding block will be

$$\boldsymbol{\omega}_{bl,i} = \boldsymbol{\omega}_{mp} \tag{32}$$

Moreover, linear velocity of the ith sliding block is given by

$$\mathbf{v}_{bl,i} = \dot{h}\mathbf{k} + \dot{b}_i\mathbf{r}_i \tag{33}$$

Substituting $\dot{h}\mathbf{k}$, $\dot{b}_i$ and $\boldsymbol{\omega}_{mp}$ from Eqs. (11), (20) and (13) into Eq. (33) and then rearranging the resultant equation lead to

$$\mathbf{v}_{bl,i} = \mathbf{J}_{bl,i}\dot{\mathbf{q}} \tag{34}$$

https://doi.org/10.1017/S0263574721000746 Published online by Cambridge University Press

where

$$\mathbf{J}_{bl,i} = \mathbf{J}_{hmp} - \frac{b_i}{\mathbf{r}_i^T \mathbf{e}_i} \begin{bmatrix} (\mathbf{r}_i \times \mathbf{e}_i)^T \mathbf{J}_{\omega mp} r_{ix} \\ (\mathbf{r}_i \times \mathbf{e}_i)^T \mathbf{J}_{\omega mp} r_{iy} \\ (\mathbf{r}_i \times \mathbf{e}_i)^T \mathbf{J}_{\omega mp} r_{iz} \end{bmatrix} \tag{35}$$

5. Dynamic modeling of the 4RPSP+PS PM

In this section, dynamic equation of 4RPSP+PS PM is derived in closed form through the Euler–Lagrange method [45]. In practice, it is desirable to define motion of a PM with regard to coordinates of the moving platform. Thus, here, we choose the four components of pose vector $\mathbf{p}$ (i.e. h, φ_x, φ_y and φ_z) as the generalized coordinates to formulate the equation of motion. Since the number of the chosen generalized coordinates is equal to the number of DOF of the manipulator, there is no need to introduce the Lagrange multipliers, [17] and the equation of motion will be achieved directly.

Since piston and cylinder of the ith RPSP leg have no relative rotational motion with respect to each other, a common coordinate frame A_i-$x_{ai}y_{ai}z_{ai}$ is considered for both of them, and attached at point A_i (Fig. 2), while the x_{ai} axis is along $\mathbf{e}_i$, z_{ai} axis is along $\mathbf{f}_i$ and y_{ai} axis is determined by the right-hand rule. The rotation matrix associated with the A_{ai}-$x_{ai}y_{ai}z_{ai}$ frame is

$$\mathbf{R}_{leg,i} = [\, \mathbf{e}_i \quad \mathbf{f}_i \times \mathbf{e}_i \quad \mathbf{f}_i \,] \tag{36}$$

For sliding block of the ith RPSP leg, a moving coordinate frame B_i-$x_{bi}y_{bi}z_{bi}$ is attached to point B_i (Fig. 2), while the x_{bi} and z_{bi} axes are along $\mathbf{r}_i$ and $\mathbf{k}_{mp}$, respectively, and y_{bi} axis is determined by the right-hand rule. Thus, the rotation matrix associated with the B_i-$x_{bi}y_{bi}z_{bi}$ frame is

$$\mathbf{R}_{bl,i} = [\, \mathbf{r}_i \quad \mathbf{k}_{mp} \times \mathbf{r}_i \quad \mathbf{k}_{mp} \,] \tag{37}$$

Hereafter, parameter m_Ω with $\Omega \in \{mp, cyl, pis, bl, pl, sc\}$ represents mass of the link Ω. Parameter $\mathbf{I}_\Omega$ is the inertia matrix of the link Ω in the fixed coordinate frame O-xyz, and $\bar{I}_\Omega$ is the inertia matrix of the link Ω in the associated local coordinate frame. The simulator cabin of the machine is considered as a body with mass m_{sc} and inertia matrices $\mathbf{I}_{sc}$ and $\bar{I}_{sc}$ in the fixed and moving coordinate frames O-xyz and C-$x_{mp}y_{mp}z_{mp}$, respectively.

5.1. Kinetic energy

The kinetic energy of the 4RPSP+PS PM is generated by all moving links, including the moving platform, the passive PS leg, proximal link, distal link and sliding block of the RPSP legs.

The moving platform and simulator cabin have a common rotational motion around the point C and a common translational motion along the z axis, so their kinetic energies are given respectably by

$$T_{mp} = \frac{1}{2} \boldsymbol{\omega}_{mp}^T \mathbf{I}_{mp} \boldsymbol{\omega}_{mp} + \frac{1}{2} m_{mp} \dot{h}^2 \mathbf{k}^T \mathbf{k} \tag{38}$$

$$T_{sc} = \frac{1}{2} \boldsymbol{\omega}_{mp}^T \mathbf{I}_{sc} \boldsymbol{\omega}_{mp} + \frac{1}{2} m_{sc} \mathbf{v}_{sc}^T \mathbf{v}_{sc} \tag{39}$$

Using the parallel axis theorem, [15] $\mathbf{I}_{mp}$ and $\mathbf{I}_{sc}$in Eqs. (38) and (39) are calculated as

$$\mathbf{I}_{mp} = \mathbf{R}_{mp} [\bar{\mathbf{I}}_{mp} + m_{mp} (\dot{h}^2 \mathbf{k}^T \mathbf{k} \mathbf{E}_3 - h^2 \mathbf{k} \mathbf{k}^T)] \mathbf{R}_{mp}^T \tag{40}$$

$$\mathbf{I}_{sc} = \mathbf{R}_{mp} [\bar{\mathbf{I}}_{sc} + m_{sc} ((h\mathbf{k} + \mathbf{d}_{sc})^T (h\mathbf{k} + \mathbf{d}_{sc}) \mathbf{E}_3 - (h\mathbf{k} + \mathbf{d}_{sc})(h\mathbf{k} + \mathbf{d}_{sc})^T)] \mathbf{R}_{mp}^T \tag{41}$$

where $\mathbf{E}_3$ is the 3×3 identity matrix. Introducing $\boldsymbol{\omega}_{mp}$, $\dot{h}\mathbf{k}$ and $\mathbf{v}_{sc}$ from Eqs. (13), (11) and (16) into Eqs. (38) and (39) results in

$$T_{mp} = \dot{\mathbf{q}}^T \mathbf{M}_{mp} \dot{\mathbf{q}} \tag{42}$$

https://doi.org/10.1017/S0263574721000746 Published online by Cambridge University Press

$$T_{sc} = \dot{\mathbf{q}}^T \mathbf{M}_{sc} \dot{\mathbf{q}} \tag{43}$$

where

$$\mathbf{M}_{mp} = \frac{1}{2}\mathbf{J}_{\omega mp}^T \mathbf{I}_{mp} \mathbf{J}_{\omega mp} + \frac{1}{2} m_{mp} \mathbf{J}_{hmp}^T \mathbf{J}_{hmp} \tag{44}$$

$$\mathbf{M}_{sc} = \frac{1}{2}\mathbf{J}_{\omega mp}^T \mathbf{I}_{sc} \mathbf{J}_{\omega mp} + \frac{1}{2} m_{sc} \mathbf{J}_{sc}^T \mathbf{J}_{sc} \tag{45}$$

The passive PS leg has a pure translational motion along the z axis, so its kinetic energy is calculated as

$$T_{pl} = \frac{1}{2} m_{pl} \dot{h}^2 \mathbf{k}^T \mathbf{k} \tag{46}$$

Substituting $\dot{h}k$ from Eq. (11) into Eq. (46) yields

$$T_{pl} = \dot{\mathbf{q}}^T \mathbf{M}_{pl} \dot{\mathbf{q}} \tag{47}$$

where

$$\mathbf{M}_{pl} = \frac{1}{2} m_{pl} \mathbf{J}_{hmp}^T \mathbf{J}_{hmp} \tag{48}$$

The ith RPSP leg rotates about unit vector $\mathbf{e}_i$. Kinetic energies of cylinder and piston of the ith RPSP leg are calculated, respectively, as

$$T_{cyl,i} = \frac{1}{2}\boldsymbol{\omega}_i^T \mathbf{I}_{cyl,i} \boldsymbol{\omega}_i + \frac{1}{2} m_{cyl} \mathbf{v}_{cyl,i}^T \mathbf{v}_{cyl,i} \tag{49a}$$

$$T_{pis,i} = \frac{1}{2}\boldsymbol{\omega}_i^T \mathbf{I}_{pis,i} \boldsymbol{\omega}_i + \frac{1}{2} m_{pis} \mathbf{v}_{pis,i}^T \mathbf{v}_{pis,i} \tag{49b}$$

Using the parallel axis theorem, $\mathbf{I}_{cyl,i}$ and $\mathbf{I}_{pis,i}$ in Eqs. (49) are calculated as

$$\mathbf{I}_{cyl,i} = \mathbf{R}_{leg,i} [\bar{\mathbf{I}}_{cyl} + m_{cyl}(\mathbf{c}_{cyl,i}^T \mathbf{c}_{cyl,i} \mathbf{E}_3 - \mathbf{c}_{cyl,i} \mathbf{c}_{cyl,i}^T)] \mathbf{R}_{leg,i}^T \tag{50a}$$

$$\mathbf{I}_{pis,i} = \mathbf{R}_{leg,i} [\bar{\mathbf{I}}_{pis} + m_{pis}(\mathbf{c}_{pis,i}^T \mathbf{c}_{pis,i} \mathbf{E}_3 - \mathbf{c}_{pis,i} \mathbf{c}_{pis,i}^T)] \mathbf{R}_{leg,i}^T \tag{50b}$$

where $\mathbf{c}_{cyl,i}$ and $\mathbf{c}_{pis,i}$ are position vectors of mass centers $c_{cyl,i}$ and $c_{pis,i}$ given, respectively, by

$$\mathbf{c}_{cyl,i} = \overrightarrow{Oc_{cyl,i}} = a\mathbf{e}_i + l_{cyl}\mathbf{f}_i \tag{51a}$$

$$\mathbf{c}_{pis,i} = \overrightarrow{Oc_{pis,i}} = a\mathbf{e}_i + (s_i - l_{pis})\mathbf{f}_i \tag{51b}$$

where l_{cyl} (l_{pis}) is the distance of mass center $c_{cyl,i}$ ($c_{pis,i}$) of cylinder (piston) of the ith RPSP leg from point A_i (B_i), see Fig. 2. By substituting $\boldsymbol{\omega}_i$, $\mathbf{v}_{cyl,i}$ and $\mathbf{v}_{pis,i}$ from Eqs. (25) and (30) into Eqs. (49), we get

$$T_{cyl,i} = \dot{\mathbf{q}}^T \mathbf{M}_{cyl,i} \dot{\mathbf{q}} \tag{52a}$$

$$T_{pis,i} = \dot{\mathbf{q}}^T \mathbf{M}_{pis,i} \dot{\mathbf{q}} \tag{52b}$$

where

$$\mathbf{M}_{cyl,i} = \frac{1}{2}\mathbf{J}_{\omega i}^T \mathbf{I}_{cyl,i} \mathbf{J}_{\omega i} + \frac{1}{2} m_{cyl} \mathbf{J}_{cyl,i}^T \mathbf{J}_{cyl,i} \tag{53a}$$

$$\mathbf{M}_{pis,i} = \frac{1}{2}\mathbf{J}_{\omega i}^T \mathbf{I}_{pis,i} \mathbf{J}_{\omega i} + \frac{1}{2} m_{pis} \mathbf{J}_{pis,i}^T \mathbf{J}_{pis,i} \tag{53b}$$

Kinetic energy of sliding block of the ith RPSP leg is given by

$$T_{bl,i} = \frac{1}{2}\boldsymbol{\omega}_{bl,i}^T \mathbf{I}_{bl,i} \boldsymbol{\omega}_{bl,i} + \frac{1}{2} m_{bl} \mathbf{v}_{bl,i}^T \mathbf{v}_{bl,i} \tag{54}$$

https://doi.org/10.1017/S0263574721000746 Published online by Cambridge University Press

with

$$\mathbf{I}_{bl,i} = \mathbf{R}_{bl,i}[\bar{\mathbf{I}}_{bl} + m_{bl}(\mathbf{c}_{bl,i}^T\mathbf{c}_{bl,i}\mathbf{E}_3 - \mathbf{c}_{bl,i}\mathbf{c}_{bl,i}^T)]\mathbf{R}_{bl,i}^T \tag{55}$$

where $\mathbf{c}_{bl,i}$ is the position vector of mass center $c_{bl,i}$ of the ith sliding block located at B_i (Fig. 2), and given by

$$\mathbf{c}_{bl,i} = \overrightarrow{OB_i} = a\mathbf{e}_i + s_i\mathbf{f}_i \tag{56}$$

Substituting $\boldsymbol{\omega}_{bl,i}$, $\mathbf{v}_{bl,i}$ and $\boldsymbol{\omega}_{mp}$ from Eqs. (32), (33) and (13) into Eq. (54) results in

$$T_{bl,i} = \dot{\mathbf{q}}^T\mathbf{M}_{bl,i}\dot{\mathbf{q}} \tag{57}$$

where

$$\mathbf{M}_{bl,i} = \frac{1}{2}\mathbf{J}_{\omega mp}^T\mathbf{I}_{bl,i}\mathbf{J}_{\omega mp} + \frac{1}{2}m_{bl}\mathbf{J}_{bl,i}^T\mathbf{J}_{bl,i} \tag{58}$$

The inertia matrices $\bar{\mathbf{I}}_{mp}$, $\bar{\mathbf{I}}_{sc}$, $\bar{\mathbf{I}}_{cyl}$, $\bar{\mathbf{I}}_{pis}$ and $\bar{\mathbf{I}}_{bl}$ and masses m_{mp}, m_{sc}, m_{pl}, m_{cyl}, m_{pis} and m_{bl} are computed using CAD model of the corresponding link in SolidWorks software. The total kinetic energy of the manipulator is

$$T_{PM} = T_{mp} + T_{sc} + T_{pl} + \sum_{i=1}^{4}\left(T_{cyl,i} + T_{pis,i} + T_{bl,i}\right) \tag{59}$$

Substituting T_{mp}, T_{sc}, T_{pl}, $T_{cyl,i}$, $T_{pis,i}$ and $T_{bl,i}$ from Eqs. (42), (43), (46), (49) and (57) into Eq. (59), and rearranging the resultant equation, yields the following expression for total kinetic energy of 4RPSP+PS PM:

$$T_{PM} = \dot{\mathbf{q}}^T\mathbf{M}(\mathbf{q})\dot{\mathbf{q}} \tag{60}$$

where $\mathbf{M}(\mathbf{q})$ is the 4×4 inertia matrix of the manipulator given as

$$\mathbf{M}(\mathbf{q}) = \mathbf{M}_{mp} + \mathbf{M}_{sc} + \mathbf{M}_{pl} + \sum_{i=1}^{4}\mathbf{M}_{cyl,i} + \sum_{i=1}^{4}\mathbf{M}_{pis,i} + \sum_{i=1}^{4}M_{bl,i} \tag{61}$$

5.2. Potential energy

Here, only the gravity force is considered as the conservative force acting on the 4RPSP+PS PM. Therefore, the potential energy stored in a link of the manipulator is defined as the amount of work required to raise mass center of the link from a horizontal reference xy plane to its current position under the influence of gravity.

Potential energies of the moving platform and the simulator cabin are calculated as

$$U_{mp} = -m_{mp}h\mathbf{g}^T\mathbf{k} \tag{62}$$

$$U_{sc} = -m_{mp}\mathbf{g}^T(h\mathbf{k} + \mathbf{d}_{sc}) \tag{63}$$

where $\mathbf{g} = [0\ 0\ -9.81]^T$ m/s^2 is the vector of gravitational acceleration. It is assumed that the passive PS leg is a uniform bar with length l_{pl}, then potential energy of this leg will be

$$U_{pl} = -m_{pl}\left(h - \frac{l_{pl}}{2}\right)\mathbf{g}^T\mathbf{k} \tag{64}$$

https://doi.org/10.1017/S0263574721000746 Published online by Cambridge University Press

Potential energies of the cylinder, piston and sliding block of the ith RPSP leg are calculated, respectively, as

$$U_{cyl,i} = -m_{cyl}\mathbf{g}^T\mathbf{c}_{cyl,i} \tag{65a}$$

$$U_{pis,i} = -m_{pis}\mathbf{g}^T\mathbf{c}_{pis,i} \tag{65b}$$

and

$$U_{bl,i} = -m_{bl}\mathbf{g}^T\mathbf{c}_{bl,i} \tag{66}$$

Hence, the total potential energy stored in the manipulator will be

$$U_{PM} = U_{mp} + U_{sc} + U_{pl} + \sum_{i=1}^{4}(U_{cyl,i} + U_{pis,i} + U_{bl,i}) = -m_{mp}h\mathbf{g}^T\mathbf{k} - m_{mp}\mathbf{g}^T(h\mathbf{k} + \mathbf{d}_{sc}) - m_{pl}\left(h - \tfrac{l_{pl}}{2}\right)\mathbf{g}^T\mathbf{k} - \sum_{i=1}^{4}\left(m_{cyl,i}\mathbf{g}^T\mathbf{c}_{cyl,i} + m_{pis,i}\mathbf{g}^T\mathbf{c}_{pis,i} + m_{bl,i}\mathbf{g}^T\mathbf{c}_{bl,i}\right) \tag{67}$$

5.3. Generalized forces

Except the gravitational and inertia forces, the generalized forces account for all other forces and moments acting on moving links of the 4RPSP+PS PM. By the principle of virtual work, [45] the vector of generalized forces $\boldsymbol{\lambda} = [\lambda_1, \lambda_2, \lambda_3, \lambda_4]^T$ of the manipulator can be formulated as

$$\boldsymbol{\lambda} = \mathcal{F}_{act} + \mathbf{J}_{PM}^{-1}\mathbf{J}_{mp}\boldsymbol{\eta}_{ext} \tag{68}$$

where $\mathcal{F}_{act} = [\mathcal{F}_1\mathcal{F}_2\mathcal{F}_3\mathcal{F}_4]^T$ is the 4×1 vector of joint forces generated by prismatic actuators, and $\boldsymbol{\eta}_{ext} = [f_{ext,z}, \mathbf{n}_{ext}]^T$ is the 4×1 vector composed of the z component of external force $\mathbf{f}_{ext} = [f_{ext,x}\ f_{ext,y}\ f_{ext,z}]^T$ and external moment $\mathbf{n}_{ext} = [n_{ext,x}\ n_{ext,y}\ n_{ext,z}]^T$ acting on the moving platform. It is worth mentioning that the frictional forces in the joints are not considered here.

5.4. Dynamic equation of the 4RPSP+PS PM

The essential step in dynamic modeling using the Lagrangian formulation is to determine the Lagrangian function, which is defined as the difference between total kinetic energy and total potential energy of the 4RPSP+PS PM, that is,

$$L_{PM} = T_{PM} - U_{PM} \tag{69}$$

Let M_{ij} be the (i, j) element of the manipulator inertia matrix $\mathbf{M}$ in Eq. (61), and $\dot{q}_i$ ($\dot{q}_j$) be the ith (jth) component of vector $\dot{\mathbf{q}}$, then we can rewrite T_{PM} in Eq. (60) as

$$T_{PM} = \sum_{i=1}^{4}\sum_{j=1}^{4} M_{ij}\dot{q}_i\dot{q}_j \tag{70}$$

Substituting T_{PM} and U_{PM} from Eqs. (60) and (67) into Eq. (70), we get

$$L_{PM} = \sum_{i=1}^{4}\sum_{j=1}^{4} M_{ij}\dot{q}_i\dot{q}_j + m_{mp}\mathbf{g}^T(h\mathbf{k} + \mathbf{d}_{sc}) + m_{pl}(h - \frac{l}{2})\mathbf{g}^T\mathbf{k} + \sum_{i=1}^{4}(m_{cyl}\mathbf{g}^T\mathbf{c}_{cyl,i} + m_{pis}\mathbf{g}^T\mathbf{c}_{pis,i} + m_{bl,i}\mathbf{g}^T\mathbf{c}_{bl,i}) \tag{71}$$

Lagrange's equations of motion are formulated for 4RPSP+PS PM in terms of the Lagrangian function [46] as follows:

$$\frac{d}{dt}\left(\frac{\partial L_{PM}}{\partial \dot{q}_i}\right) - \frac{\partial L_{PM}}{\partial q_i} = \lambda_i, \quad i = 1, 2, 3, 4 \tag{72}$$

https://doi.org/10.1017/S0263574721000746 Published online by Cambridge University Press

Thus, the terms included in above equation should be calculated. Since the potential energy does not depend on $\dot{q}_i$, taking partial derivative of Eq. (71) with respect to $\dot{q}_i$ yields

$$\frac{\partial L_{PM}}{\partial \dot{q}_i} = \sum_{j=1}^{4} M_{ij}\dot{q}_j \tag{73}$$

Taking total derivative of Eq. (73) with respect to time gives

$$\frac{d}{dt}\left(\frac{\partial L_{PM}}{\partial \dot{q}_i}\right) = \sum_{j=1}^{4} M_{ij}\ddot{q}_j + \sum_{j=1}^{4}\left(\frac{dM_{ij}}{dt}\right)\dot{q}_j = \sum_{j=1}^{4} M_{ij}\ddot{q}_j + \sum_{j=1}^{4}\sum_{k=1}^{4}\frac{\partial M_{ij}}{\partial x_k}\dot{q}_k\dot{q}_j \tag{74}$$

Taking partial derivative of Eq. (71) with respect to q_i yields

$$\begin{aligned}\frac{\partial L_{PM}}{\partial q_i} &= \frac{\partial}{\partial x_i}\sum_{j=1}^{4}\sum_{k=1}^{4} M_{jk}\dot{q}_j\dot{q}_k + (m_{mp}+m_{pl})\left(\frac{\partial h}{\partial q_i}\right)\mathbf{g}^T\mathbf{k} \\ &+ \sum_{j=1}^{4}\left(m_{cyl}\mathbf{g}^T\left(\frac{\partial \mathbf{c}_{cyl,j}}{\partial q_i}\right) + m_{pis}\mathbf{g}^T\left(\frac{\partial \mathbf{c}_{pis,j}}{\partial q_i}\right) + m_{bl}\mathbf{g}^T\left(\frac{\partial \mathbf{c}_{bl,j}}{\partial q_i}\right)\right)\end{aligned} \tag{75}$$

By substituting Eqs. (74) and (75) into (72), we get

$$\sum_{j=1}^{4} M_{ij}\ddot{q}_j + \sum_{j=1}^{4}\sum_{k=1}^{4}\left(\frac{\partial M_{ij}}{\partial q_k} - \frac{\partial M_{jk}}{\partial q_i}\right)\dot{q}_k\dot{q}_j + \delta_i = \lambda_i \tag{76}$$

where

$$\delta_i = (m_{mp}+m_{pl})\left(\frac{\partial h}{\partial q_i}\right)\mathbf{g}^T\mathbf{k} + \sum_{j=1}^{4}\left(m_{cyl}\mathbf{g}^T\left(\frac{\partial \mathbf{c}_{cyl,j}}{\partial q_i}\right) + m_{pis}\mathbf{g}^T\left(\frac{\partial \mathbf{c}_{pis,j}}{\partial q_i}\right) + m_{bl}\mathbf{g}^T\left(\frac{\partial \mathbf{c}_{bl,j}}{\partial q_i}\right)\right) \tag{77}$$

Writing Eq. (76) for i = 1, 2, 3, 4, and casting the resultant equations into a matrix form gives

$$\mathbf{M}(\mathbf{q})\ddot{\mathbf{q}} + \mathbf{N}(\mathbf{q},\dot{\mathbf{q}})\dot{\mathbf{q}} + \boldsymbol{\delta}(\mathbf{q}) = \boldsymbol{\lambda} \tag{78}$$

where vector $\boldsymbol{\delta}(\mathbf{q}) = [\delta_1, \delta_2, \delta_3, \delta_4]^T$ is the 4×1 vector of gravity forces, and $\mathbf{N}(\mathbf{q},\dot{\mathbf{q}})$ is

$$\mathbf{N}(\mathbf{q},\dot{\mathbf{q}}) = \begin{bmatrix} \dot{\mathbf{q}}^T\mathbf{n}_{11} & \dot{\mathbf{q}}^T\mathbf{n}_{12} & \dot{\mathbf{q}}^T\mathbf{n}_{13} & \dot{\mathbf{q}}^T\mathbf{n}_{14} \\ \dot{\mathbf{q}}^T\mathbf{n}_{21} & \dot{\mathbf{q}}^T\mathbf{n}_{22} & \dot{\mathbf{q}}^T\mathbf{n}_{23} & \dot{\mathbf{q}}^T\mathbf{n}_{24} \\ \dot{\mathbf{q}}^T\mathbf{n}_{31} & \dot{\mathbf{q}}^T\mathbf{n}_{32} & \dot{\mathbf{q}}^T\mathbf{n}_{33} & \dot{\mathbf{q}}^T\mathbf{n}_{34} \\ \dot{\mathbf{q}}^T\mathbf{n}_{41} & \dot{\mathbf{q}}^T\mathbf{n}_{42} & \dot{\mathbf{q}}^T\mathbf{n}_{43} & \dot{\mathbf{q}}^T\mathbf{n}_{44} \end{bmatrix}_{4\times 4} \tag{79}$$

where the 4×1 vectors $\mathbf{n}_{ij}$ (i, j = 1, 2, 3, 4) is given by

$$\mathbf{n}_{ij} = \left[\left(\frac{\partial M_{ij}}{\partial q_1} - \frac{\partial M_{j1}}{\partial q_i}\right) \quad \left(\frac{\partial M_{ij}}{\partial q_2} - \frac{\partial M_{j2}}{\partial q_i}\right) \quad \left(\frac{\partial M_{ij}}{\partial q_3} - \frac{\partial M_{j3}}{\partial q_i}\right) \quad \left(\frac{\partial M_{ij}}{\partial q_4} - \frac{\partial M_{j4}}{\partial q_i}\right)\right]^T \tag{80}$$

In fact, $\mathbf{N}(\mathbf{q},\dot{\mathbf{q}})$ is a 4×4 matrix representing Coriolis and centrifugal accelerations of the manipulator moving links. By substituting the value of $\boldsymbol{\lambda}$ from Eq. (68) into Eq. (78), we obtain the closed-form dynamic equation of 4RPSP+PS PM in terms of $\dot{\mathbf{q}}$ and $\ddot{\mathbf{q}}$ as follows:

$$\mathbf{M}(\mathbf{q})\ddot{\mathbf{q}} + \mathbf{N}(\mathbf{q},\dot{\mathbf{q}})\dot{\mathbf{q}} + \boldsymbol{\delta}(\mathbf{q}) = \mathcal{F}_{act} + \mathbf{J}_{PM}^{-1}\mathbf{J}_{mp}\boldsymbol{\eta}_{mp} \tag{81}$$

The matrices $\mathbf{M}(\mathbf{q})$, $\mathbf{N}(\mathbf{q},\dot{\mathbf{q}})$, $\mathbf{J}_{PM}^{-1}\mathbf{J}_{mp}$ and also vector $\boldsymbol{\delta}(\mathbf{q})$ in Eq. (81) can be calculated easily, because they only depend on $\mathbf{q}$ and $\dot{\mathbf{q}}$, and on known architectural parameters of the manipulator.

6. Global power transmission index

The total input power, P_{input}, of the 4RPSP+PS PM equals sum of the three mechanical-typed powers: (1) the useful power, P_{useful}, consumed by the moving platform, the PS leg and the simulator cabin, (2)

https://doi.org/10.1017/S0263574721000746 Published online by Cambridge University Press

the loss power, P_{loss}, caused by friction, (3) the time rate of the energy consumed by R$\underline{\text{P}}$SP legs, that is, the transmission power, P_{trans}, of the manipulator. Namely,

$$P_{\text{input}} = P_{\text{useful}} + P_{\text{loss}} + P_{\text{trans}} \tag{82}$$

As mentioned before, friction forces are neglected in this study, so $P_{loss} = 0$. In a high speed operation process, the potential energy of the manipulator is ignorable with respect to its kinematic energy. Thus, here, we only focus on time rate of the kinetic energy and influence of the gravity is not considered. The energy efficiency of 4R$\underline{\text{P}}$SP+PS PM based on the energy consumed by active R$\underline{\text{P}}$SP legs is [43]:

$$\eta_e = \frac{P_{\text{useful}}}{P_{\text{input}}} = 1 - \frac{P_{\text{trans}}}{P_{\text{input}}} \tag{83}$$

The transmission power P_{trans} of the manipulator is calculated by the following relation:

$$P_{\text{trans}} = \sum_{i=1}^{4} \frac{dT_{cyl,i}}{dt} + \sum_{i=1}^{4} \frac{dT_{pis,i}}{dt} + \sum_{i=1}^{4} \frac{dT_{bl,i}}{dt} \tag{84}$$

where the time rates of kinetic energies of the cylinder, piston and sliding block of the ith R$\underline{\text{P}}$SP leg are obtained from Eqs. (57) and (52) in terms of velocity $\dot{\mathbf{q}}$ and acceleration $\ddot{\mathbf{q}} = [\,\ddot{h}\ \ddot{\varphi}_x\ \ddot{\varphi}_y\ \ddot{\varphi}_z\,]^T$ of the moving platform as follows:

$$\frac{dT_{cyl,i}}{dt} = \ddot{\mathbf{q}}^T \mathbf{M}_{cyl,i}\dot{\mathbf{q}} + \dot{\mathbf{q}}^T \dot{\mathbf{M}}_{cyl,i}\dot{\mathbf{q}} + \dot{\mathbf{q}}^T \mathbf{M}_{cyl,i}\ddot{\mathbf{q}} \tag{85a}$$

$$\frac{dT_{pis,i}}{dt} = \ddot{\mathbf{q}}^T \mathbf{M}_{pis,i}\dot{\mathbf{q}} + \dot{\mathbf{q}}^T \dot{\mathbf{M}}_{pis,i}\dot{\mathbf{q}} + \dot{\mathbf{q}}^T \mathbf{M}_{pis,i}\ddot{\mathbf{q}} \tag{85b}$$

$$\frac{dT_{bl,i}}{dt} = \ddot{\mathbf{q}}^T \mathbf{M}_{bl,i}\dot{\mathbf{q}} + \dot{\mathbf{q}}^T \dot{\mathbf{M}}_{bl,i}\dot{\mathbf{q}} + \dot{\mathbf{q}}^T \mathbf{M}_{bl,i}\ddot{\mathbf{q}} \tag{85c}$$

The sign of P_{trans} in Eq. (84) shows variation trend of kinetic energy of the R$\underline{\text{P}}$SP legs. When it is positive, the kinetic energy of the legs increases and negative sign indicates that the kinetic energy decreases, meaning that it does work on actuators, moving platform or both.

Equations (85) reveals that the time rates of kinetic energies of R$\underline{\text{P}}$SP legs depend on the velocity $\dot{\mathbf{q}}$ and acceleration $\ddot{\mathbf{q}}$ of the moving platform. According to Eq. (83), the minimum value of energy efficiency of the manipulator (i.e. $\eta_e = 0$) occurs when $P_{trans} = P_{input}$. On this condition, the energy from actuators is only used to change kinestate (i.e. velocity and acceleration) of R$\underline{\text{P}}$SP legs, and kinetic energy of the moving platform remains unchanged. Thus, the moving platform moves at a constant velocity ($\ddot{\mathbf{q}} = 0$), and Eqs. (85) are summarized to

$$\frac{dT_{cyl,i}}{dt} = \dot{\mathbf{q}}^T \dot{\mathbf{M}}_{cyl,i}\dot{\mathbf{q}} \tag{86a}$$

$$\frac{dT_{pis,i}}{dt} = \dot{\mathbf{q}}^T \dot{\mathbf{M}}_{pis,i}\dot{\mathbf{q}} \tag{86b}$$

$$\frac{dT_{bl,i}}{dt} = \dot{\mathbf{q}}^T \dot{\mathbf{M}}_{bl,i}\dot{\mathbf{q}} \tag{86c}$$

Introducing Eqs. (86) into Eq. (84), we get transmission power of the 4R$\underline{\text{P}}$SP+PS PM as

$$P_{\text{trans}} = \sum_{i=1}^{4} \dot{\mathbf{q}}^T (\dot{\mathbf{M}}_{cyl,i} + \dot{\mathbf{M}}_{pis,i} + \dot{\mathbf{M}}_{bl,i})\dot{\mathbf{q}} \tag{87}$$

When velocity magnitude of the moving platform, $\|\dot{\mathbf{q}}\|$, varies, P_{trans} changes proportionally for all points in the workspace of the manipulator. Thus, in order to compute P_{trans}, one can take a constant value for velocity magnitude of the moving platform as $\|\dot{\mathbf{q}}\| = D$. Apart from the velocity magnitude,

https://doi.org/10.1017/S0263574721000746 Published online by Cambridge University Press

$\boldsymbol{P}_{trans}$ is also affected by velocity direction of the moving platform significantly. The velocity direction, for which the P_{trans} becomes maximal at a specific point, is obtained through solving the following system of equations:

$$\begin{cases} \nabla(P_{\max}) = \lambda \nabla(\dot{h}^2 + \dot{\varphi}_x^2 + \dot{\varphi}_y^2 + \dot{\varphi}_z^2) \\ \dot{h}^2 + \dot{\varphi}_x^2 + \dot{\varphi}_y^2 + \dot{\varphi}_z^2 = \|\dot{\mathbf{q}}\|^2 = D^2 \end{cases} \tag{88}$$

where $\nabla(\cdot)$ denotes gradient of function $(\cdot)$ with respect to $(\dot{h}, \dot{\varphi}_x, \dot{\varphi}_y, \dot{\varphi}_z)$, and λ is the Lagrange multiplier. Equation (88) is, in fact, a system of five equations in five unknowns $\dot{h}$, $\dot{\varphi}_x$, $\dot{\varphi}_y$, $\dot{\varphi}_z$ and λ, that are

$$\begin{cases} \frac{\partial P_{\max}}{\partial \dot{h}} - 2\lambda \dot{h} = 0 \\ \frac{\partial P_{\max}}{\partial \dot{\varphi}_x} - 2\lambda \dot{\varphi}_x = 0 \\ \frac{\partial P_{\max}}{\partial \dot{\varphi}_y} - 2\lambda \dot{\varphi}_y = 0 \\ \frac{\partial P_{\max}}{\partial \dot{\varphi}_z} - 2\lambda \dot{\varphi}_z = 0 \\ \dot{h}^2 + \dot{\varphi}_x^2 + \dot{\varphi}_y^2 + \dot{\varphi}_z^2 - D^2 = 0 \end{cases} \tag{89}$$

On this basis, a local power transmission index is defined as

$$\lambda_{\text{pt}} = \max\left(|P_{\text{trans}}| \right) \tag{90}$$

where λ_{pt} denotes the maximum value of P_{trans} for different velocity directions of the moving platform at a specific point in the workspace. The less the index, the less the energy the RPSP legs need for self-motion, and energy efficiency η_e of the manipulator will be higher. Figure 4 shows distribution of λ_{pt} for three arbitrary sets of α, φ_z at h = 1 m. The values of required architectural and dynamic parameters of the manipulator are given in Appendix A. As shown in Fig. 4, λ_{pt} has a less value especially at the central region of the workspaces and becomes larger when approaching the workspace boundaries. The singular configuration of the manipulator occurs when RPSP legs are parallel with the central PS leg, and $\alpha = \pi/4$ [44]. In this configuration, the input power of the manipulator is completely consumed by the RPSP legs (i.e., $P_{trans} = P_{input}$). Consequently, for $\alpha = \pi/4$, $\eta_e = 0$ and λ_{pt} becomes so large (Fig. 4).

Since λ_{pt} is a pose-dependent index, in order to evaluate energy efficiency of the 4RPSP+PS PM in the whole workspace, a global power transmission index is proposed [43].

$$\Gamma_{\text{pt}} = \frac{\int_w \lambda_{\text{pt}} dw}{\int_w dw} \tag{91}$$

where w denotes total 4D workspace of the manipulator in $(h, \varphi_x, \varphi_y, \varphi_z)$ space. The less the value of Γ_{pt}, the more energy efficient the manipulator will be in its corresponding workspace. On the other hand, since λ_{pt} is obtained on the worst condition with maximum P_{trans}, the index Γ_{pt} can be utilized as a criterion for design optimization of the manipulator, regardless of trajectory or kinestate of the moving platform. Note that, for the given dynamic properties of the manipulator, λ_{pt} in Eq. (90) and consequently Γ_{pt} in Eq. (91) depend only on two architectural parameters of the manipulator that are a and α.

7. Power optimization of the 4RPSP+PS PM

The main problem is to find the best design of the 4RPSP+PS PM with maximal workspace volume, V_T, and minimal Γ_{pt} over the workspace. The common method to solve this problem is to find a minimum value of a single objective function which is a weighted sum of the two criteria $1/V_T$ and Γ_{pt}. In ref. [44], it was shown that the minimum value of $1/V_T$ occurs when $\alpha = \pi/4$. But, as shown in Fig. 4, the maximum values of Γ_{pt} occurs at the same value of α. Therefore, there is a converse relation between the values of the two criteria, and it is more reasonable to minimize them through a multiobjective optimization problem and to find a Pareto front of optimal solutions, instead of a single solution.

https://doi.org/10.1017/S0263574721000746 Published online by Cambridge University Press

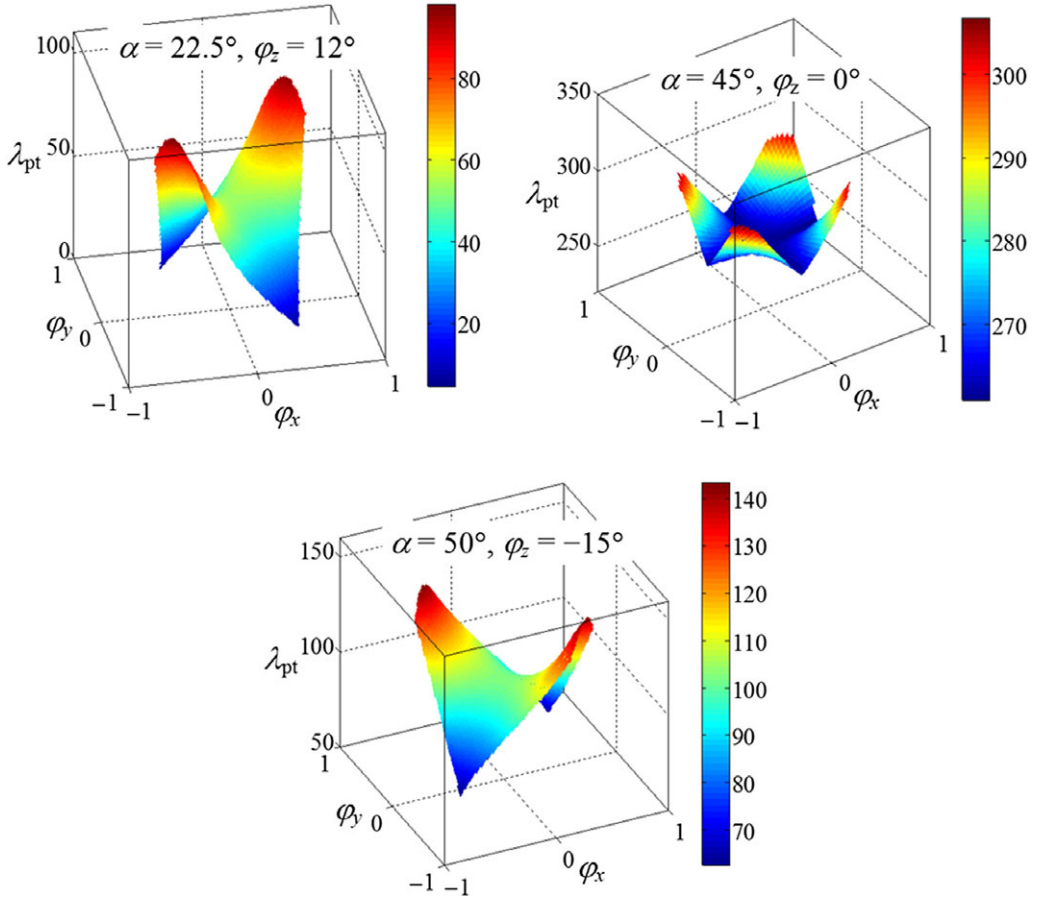

Figure 4. *λ_{pt} of the 4RPSP+PS PM for three arbitrary sets of α and φ_z at h =1 m.*

Let h_{min} and h_{max} be the minimum and maximum values of h for which the manipulator has orientation workspaces in $(\varphi_x, \varphi_y, \varphi_z)$ space. Through discretizing each orientation workspace in k elements, volume of total workspace of the manipulator is defined as the summation of volumes of the orientation workspaces [44]:

$$V_T = \sum_{i=1}^{n} \sum_{j=1}^{k} \Delta V_{ij} \tag{92}$$

where n is the number of equally distant points between h_{min} and h_{max}, and

$$\Delta V_{ij} = \Delta\varphi_{x,ij} \Delta\varphi_{y,ij} \Delta\varphi_{z,ij} \tag{93}$$

is the volume of the jth element (j = 1, 2, …, k) in the ith orientation workspace (i = 1, 2, …, n). The above global power transmission index Γ_{pt} and V_T will be used as two functions to define a multiobjective optimization problem as follows:

$$\text{Minimize } g_1(\mathbf{x}) = 1/V_T \tag{94a}$$

$$\text{Minimize } g_2(\mathbf{x}) = \Gamma_{pt} \tag{94b}$$

Over the design parameters:

$$\mathbf{x} = [a, \alpha] \tag{95}$$

and subject to the following kinematic constraints [44]:

https://doi.org/10.1017/S0263574721000746 Published online by Cambridge University Press

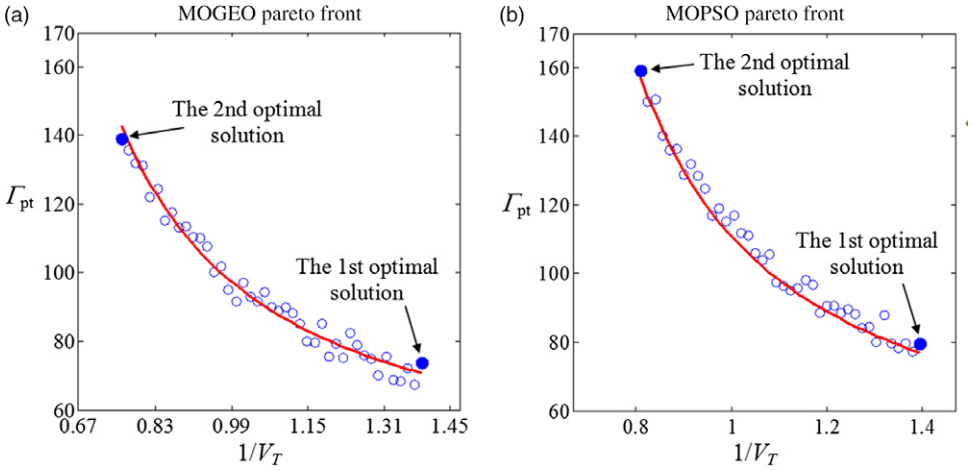

Figure 5. *Pareto fronts of (a) MOGEO and (b) MOPSO for the multiobjective optimization problem.*

Radius of base circle:

$$a_{\min} \leq a \leq a_{\max} \tag{96a}$$

Angle between axes of passive P joints:

$$0 \leq \alpha \leq \pi/2 \tag{96b}$$

The actuators stroke:

$$s_{\min} \leq s_i \leq s_{\max} \tag{96c}$$

Motion range of the passive spherical joints:

$$0 \leq \cos^{-1}(\mathbf{k}^T \mathbf{k}_{mp}) \leq \gamma_{\max} \tag{96d}$$

$$0 \leq \cos^{-1}(\mathbf{f}_i^T \mathbf{k}_{mp}) \leq \gamma_{\max} \tag{96e}$$

Range of the passive prismatic joints:

$$0 \leq b_i \leq b_{\max} \tag{96f}$$

Kinematic conditioning index (KCI):

$$\text{KCI} \geq 0.3 \tag{96g}$$

where KCI is the ratio of the smallest to the largest singular values of the Jacobian matrix $\mathbf{J}_{PM}$ [44]. The larger the KCI, the farther the manipulator is from singularities. The values of lower and upper bounds of the constraints are given as $a_{min} = 0.45$ m, $a_{max} = 1.5$ m, $s_{min} = 1.8$ m, $s_{max} = 2.2$ m, $\gamma_{max} = 40°$ and $b_{max} = 1.1$ m.

Mohammadi-Balani et al. [47] have recently introduced a novel swarm-intelligence metaheuristic algorithm called golden eagle optimizer (GEO) that is based on golden eagles' hunting process. GEO is founded on intelligent adjustments of attack and cruise propensities that golden eagles perform while searching for prey and hunting. They also extend GEO to multiobjective golden eagle optimizer (MOGEO) to solve multiobjective optimization problems.

Here, we utilize MOGEO to solve formulated optimization problem in Eq. (94). The resulting Pareto front of the solutions is shown in Fig. 5(a), revealing that the larger the manipulator workspace, the larger the value of Γ_{pt} (and consequently the smaller η_e) for the obtained solutions (or optimal designs). In order to compare the solutions, two optimal designs are selected from both ends of the Pareto front, as shown by blue solid points in Fig. 5(a). Values of design parameters and objective functions for the

https://doi.org/10.1017/S0263574721000746 Published online by Cambridge University Press

Table I. *Values of design parameters, objective functions, η_V and η_Γ for the selected optimal designs.*

Variables	1st optimal design by MOGEO	2nd optimal design by MOGEO	1st optimal design by MOPSO	2nd optimal design by MOPSO	Non-optimal design
a [m]	0.83	0.96	0.84	0.99	0.5
α [rad]	0.46	0.69	0.45	0.70	$\pi/4$
$1/V_T$	1.39	0.76	1.395	0.81	0.49
Γ_{pt}	73.9	139.6	79.69	159.3	284.41
$\eta_V \times 100$	64.70	35.5	64.87	39.50	–
$\eta_\Gamma \times 100$	74.0	50.9	71.98	43.98	–

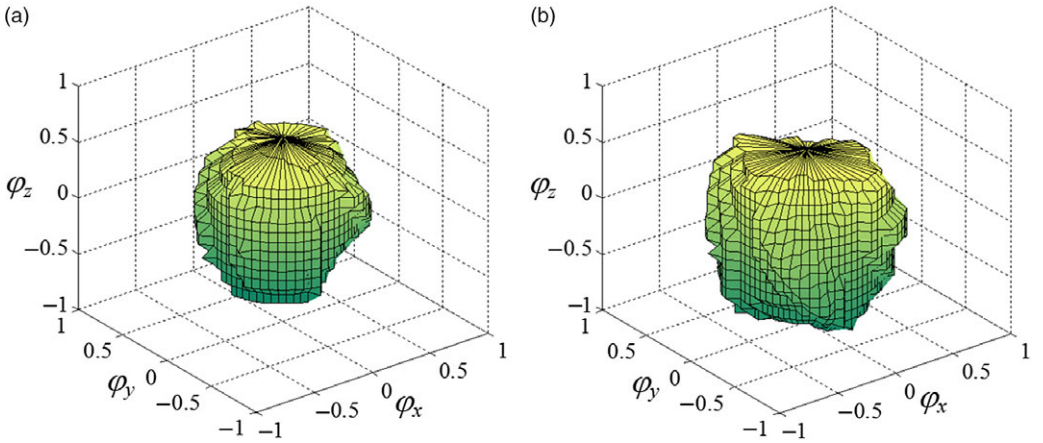

Figure 6. *The 3D orientation workspaces of (a) the 1st optimal design and (b) the 2nd optimal design at $h = 1$ m.*

selected optimal designs and also for a reference non-optimal design are listed in Table I, and their 3D orientation workspaces are plotted in Fig. 6 at an arbitrary value of $h = 1$ m. As well, λ_{pt} of the selected optimal designs are plotted in Figs. 7 and 8 at three arbitrary values of h and φ_z. It can be observed from Table I and Figs. 6, 7 and 8 that the value of Γ_{pt} for the 1st optimal design is lower than that of the 2nd optimal design, while the volume of total workspace of the 2nd optimal design is larger than that of the 1st design. In other words, the 1st optimal design is a more energy efficient manipulator, but with smaller workspace. In Table I, the variables η_V and η_Γ are defined as

$$\eta_V = \left| \frac{V_{T,opt} - V_{T,non-opt}}{V_{T,non-opt}} \right| \tag{97a}$$

$$\eta_\Gamma = \left| \frac{\Gamma_{pt,opt} - \Gamma_{pt,non-opt}}{\Gamma_{pt,non-opt}} \right| \tag{97b}$$

where $V_{T,non-opt}$ and $V_{T,opt}$ denote volumes of total workspaces of the reference non-optimal design and of the 1st and 2nd optimal designs, respectively. Moreover, $\Gamma_{pt,non-opt}$ and $\Gamma_{pt,opt}$ denote Γ_{pt}s of the reference non-optimal design and of the 1st and 2nd optimal designs, respectively. In fact, η_V and η_Γ show relative variations of V_T and Γ_{pt} of the optimal designs with respect to the reference non-optimal design, respectively. The values of η_V and η_Γ in Table I reveal that V_T of the 1st and the 2nd optimal designs are 64.7% and 35.5% less than that of the reference non-optimal design, respectively, but Γ_{pt} of those optimal designs are 74% and 50.9% lower than that of the reference non-optimal design,

https://doi.org/10.1017/S0263574721000746 Published online by Cambridge University Press

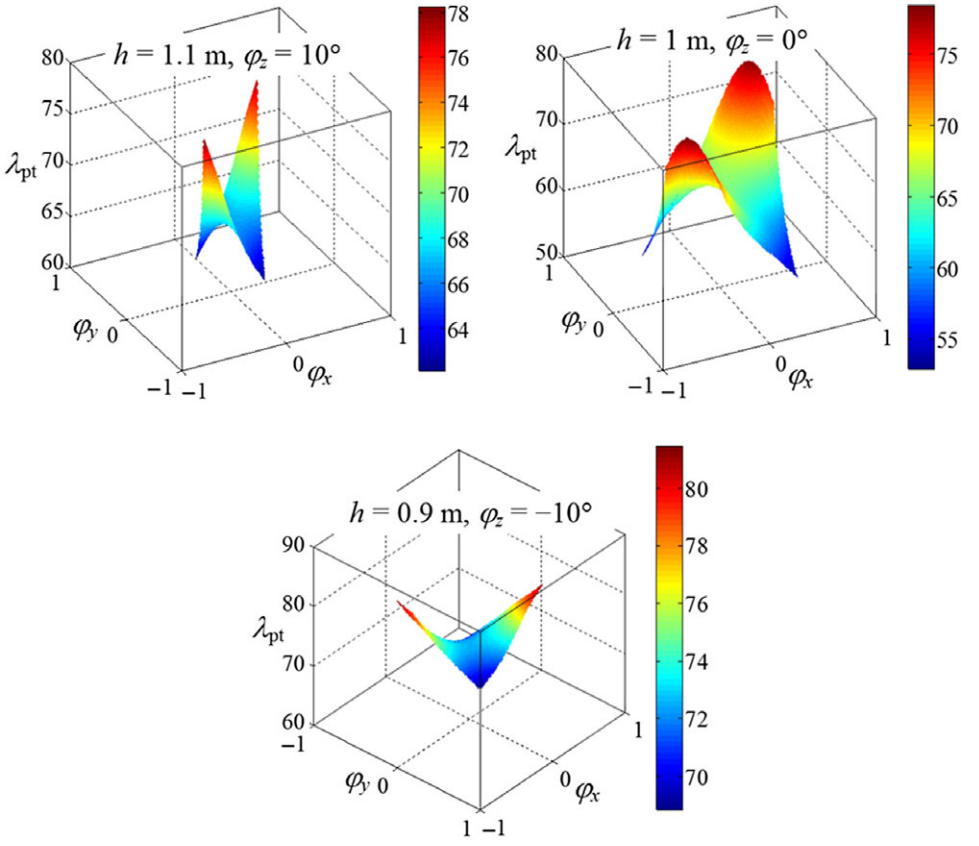

Figure 7. *λ_{pt} of the 1st optimal design for three arbitrary sets of h and φ_z.*

respectively. As a consequence, all the optimal solutions in the Pareto front of MOGEO (Fig. 5(a)) are more energy efficient than the reference non-optimal design, and a designer can easily select his/her favorite design from the Pareto front, based on the desired values of Γ_{pt} and V_T.

Moreover, to show efficiency of MOGEO, the above optimization problem is also solved by the classical multiobjective particle swarm optimization (MOPSO) [48]. The resulting Pareto front of the solutions is shown in Fig. 5(b). Similarly, two optimal designs are selected from both ends of this Pareto front, as shown by blue solid points in Fig. 5(b). Values of the corresponding design parameters and objective functions are listed in Table I. But, by comparison between Figs. 5(a) and (b) and also between the 1st and the 2nd solutions of the two methods in Table I, one can find that the solutions obtained by MOGEO method are non-dominated by those derived through MOPSO method. The optimization is run on Intel (R) Pentium CPU G3250 with 4.00 GB RAM. Computational times of running MOGEO and MOPSO for this problem are 26.15 and 23.31 s with 500 iterations, respectively. Consequently, although MOGEO converges to the optimal solutions more slowly, it can find optimal designs of the manipulator with higher V_T's and lower Γ_{pt}'s than MOPSO.

7.1. Numerical example

To show efficiency of the above methodology, a numerical example with a given trajectory is presented to compare consumed powers of two optimal designs obtained in the previous section using MOGEO. Except for the design parameters a and α, values of other architectural and dynamic parameters of

https://doi.org/10.1017/S0263574721000746 Published online by Cambridge University Press

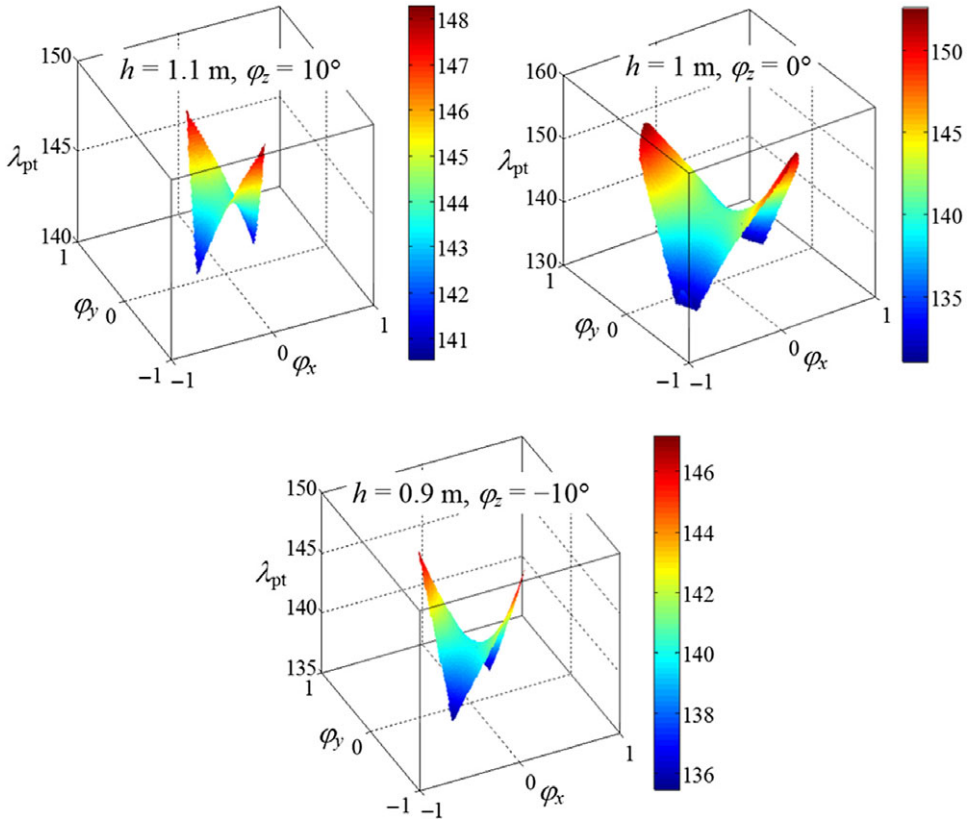

Figure 8. *λ_{pt} of the 2nd optimal design for three arbitrary sets of h and φ_z.*

the 4RPSP+PS PM are taken from Appendix A. Dynamics of the manipulator is also simulated using SimMechanics toolbox of Matlab software. Time trajectory of the moving platform is given as follows:

$$h(t) = 1.2(\sin(0.2t) + 0.8\cos(0.2t))\ m \tag{98a}$$

$$\varphi_x(t) = 0.37 + 0.1\cos(t) \tag{98b}$$

$$\varphi_y(t) = 0.2(\cos(0.2t) - 0.4\sin(t)) + 0.3 \tag{98c}$$

$$\varphi_z(t) = 0.1\sin(t) + 0.4 \tag{98d}$$

where $0 \le t \le 2\pi$ s. To compute input power of the manipulator, at first, its inverse dynamics is analyzed. In inverse dynamic analysis, the actuator forces $\mathcal{F}_{act}$ are calculated for the given trajectory, $\mathbf{q}(t) = [h(t)\ \varphi_1(t)\ \varphi_2(t)\ \varphi_3(t)]^T$, of the moving platform. To this aim, Eq. (81) is rewritten as

$$\mathcal{F}_{act} = \mathbf{M}(\mathbf{q})\ddot{\mathbf{q}} + \mathbf{N}(\mathbf{q}, \dot{\mathbf{q}})\dot{\mathbf{q}} + \boldsymbol{\delta}(\mathbf{q}) - \mathbf{J}_{PM}^{-1}\mathbf{J}_{mp}\boldsymbol{\eta}_{mp} \tag{99}$$

The actuator velocities $\dot{s}_i$ and their forces $\mathcal{F}_i$ are calculated for the two selected optimal designs presented above using Eqs. (29) and (99). The actuator velocities and forces are plotted in Figs. 9 and 10. Consequently, the instantaneous required driving power of the ith actuator will be

$$P_{\text{input},i} = \mathcal{F}_i\dot{s}_i \tag{100}$$

and the total input power of the four actuators is

$$P_{\text{input}} = \sum_{i=1}^{4} P_{\text{input},i} \tag{101}$$

https://doi.org/10.1017/S0263574721000746 Published online by Cambridge University Press

Table II. *The maximum and minimum values of input powers for the two selected optimal designs.*

Selected designs	$P_{input,max}$ [W]	$P_{input,min}$ [W]
The 1st optimal design	220.7	−176.4
The 2nd optimal design	588.6	−450.9

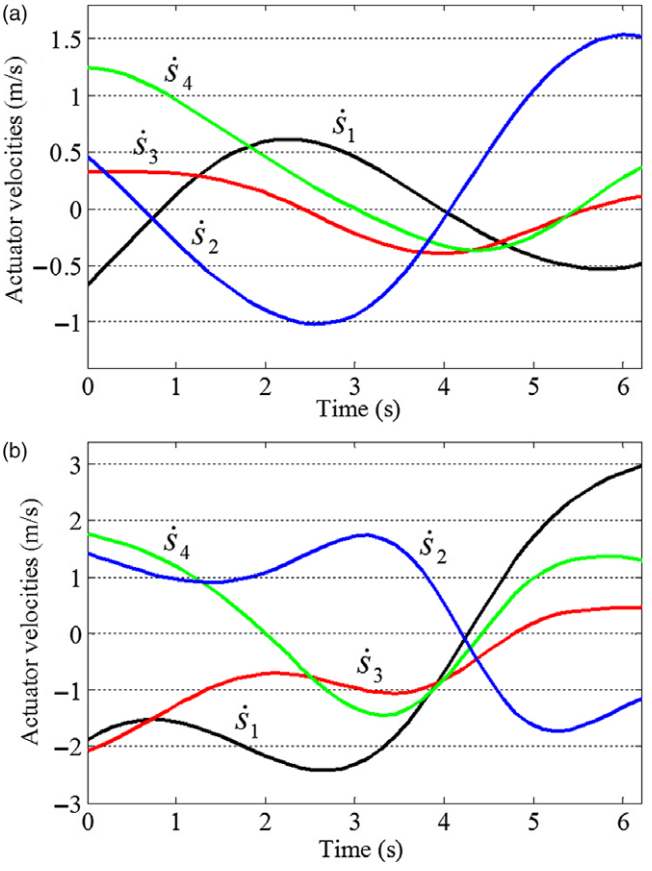

Figure 9. *The actuator velocities of 4RPSP+PS PM for (a) the 1st optimal design and (b) the 2nd optimal design obtained by MOGEO.*

The values of $P_{input,i}$ and P_{input} along the given trajectory are plotted in Figs. 11 and 12 for the two optimal designs. Note that the negative values of driving input powers in Figs. 11 and 12 are due to the negative values of actuator velocities $\dot{s}_i$ in Eq. (100) during motion. However, for computing energy efficiency of the manipulator (Eq. (83)), the absolute values of P_{input} are used. The maximum and minimum values of actuator input powers during the motion are given in Table II for the two designs.

It is clear from Fig. 12 and Table II that the required power of the 1st optimal design is much less than that of the 2nd optimal design for the given trajectory. Although the values of actuator forces for the both designs are approximately equal (Fig. 10), the actuators move more slowly for the 1st optimal design compared to the 2nd one (Fig. 9). This leads to a less P_{input} of the 1st optimal design. Next, the forward dynamic analysis of the manipulator is analyzed. In forward dynamic analysis, the actuator forces $\mathcal{F}_{act}$ calculated in previous step for the two optimal designs, initial pose and initial velocity of the moving

https://doi.org/10.1017/S0263574721000746 Published online by Cambridge University Press

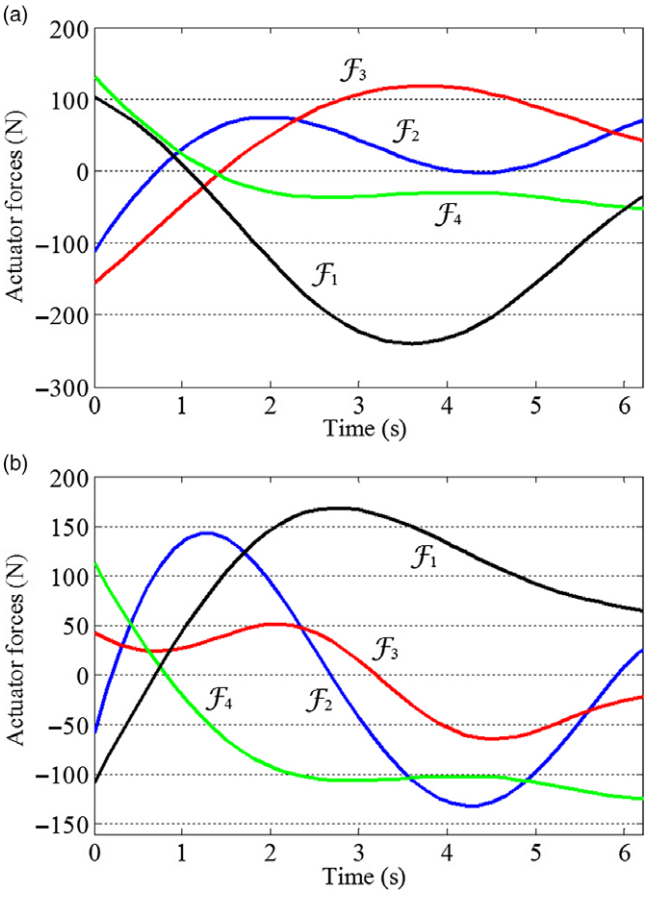

Figure 10. *The actuator forces of 4RPSP+PS PM for (a) the 1st optimal design and (b) the 2nd optimal design obtained by MOGEO.*

platforms are given and the problem is to find resulting motion of the moving platform. To this aim, we rewrite Eq. (81) as

$$\ddot{\mathbf{q}} = \mathbf{M}^{-1}(\mathbf{q})(\mathcal{F}_{act} + \mathbf{J}_{PM}^{-1}\mathbf{J}_{mp}\boldsymbol{\eta}_{mp} - \mathbf{N}(\mathbf{q}, \dot{\mathbf{q}})\dot{\mathbf{q}} - \boldsymbol{\delta}(\mathbf{q})) \tag{102}$$

Initial pose and velocity of the moving platform are obtained from the given time trajectory of the moving platform (Eqs. (98)) as follows:

$$\mathbf{q}(0) = [\,0.96 \quad 0.47 \quad 0.5 \quad 0.4\,]^T \tag{103a}$$

$$\dot{\mathbf{q}}(0) = [\,0.24 \quad 0.0 \quad -0.08 \quad 0.1\,]^T \tag{103b}$$

Using the above data, the value of $\ddot{\mathbf{q}}$ is computed through Eq. (102), and then $\ddot{\mathbf{q}}$ is integrated to calculate new values of $\dot{\mathbf{q}}$ and $\mathbf{q}$. This process is repeated for $t = 0$ to 2π to obtain time trajectory of the moving platform. The calculated time trajectories for the two optimal designs along with the given one (Eqs. (98)) are presented in Figs. 13 and 14. One can see that the given and calculated trajectories of the moving platform are indistinguishable, that is to say, the obtained output of forward dynamic analysis is coincident with the given input of inverse dynamic analysis. Moreover, both of the optimal designs give the same time trajectory of the moving platform. SimMechanics model for the forward dynamics of the 4RPSP+PS PM is shown in Fig. 15. The trajectories of the moving platform obtained by the SimMechanics model are also shown in Figs. 13 and 14 that are so close to two previous mathematical

https://doi.org/10.1017/S0263574721000746 Published online by Cambridge University Press

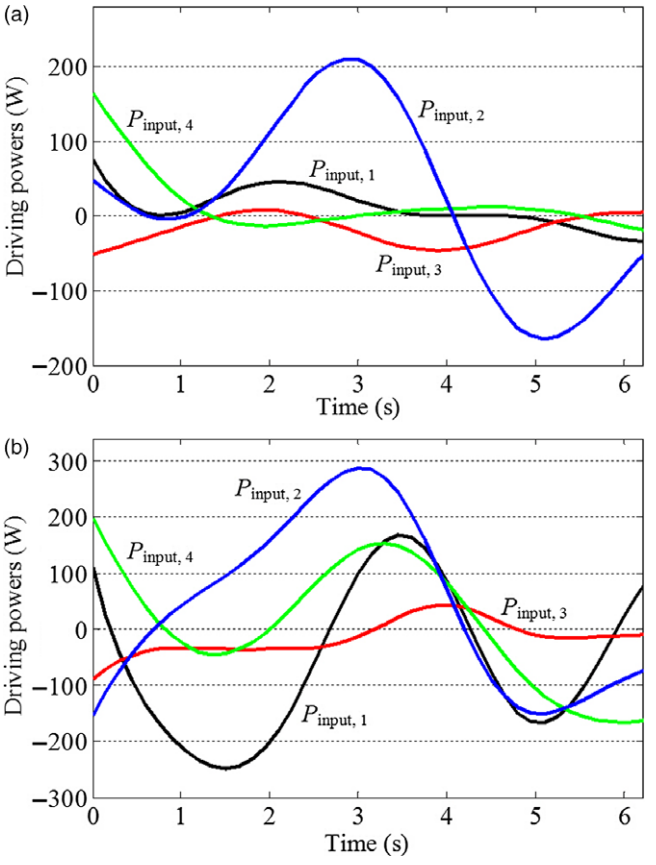

Figure 11. *The driving power of actuators for (a) the 1st optimal design and (b) the 2nd optimal design obtained by MOGEO.*

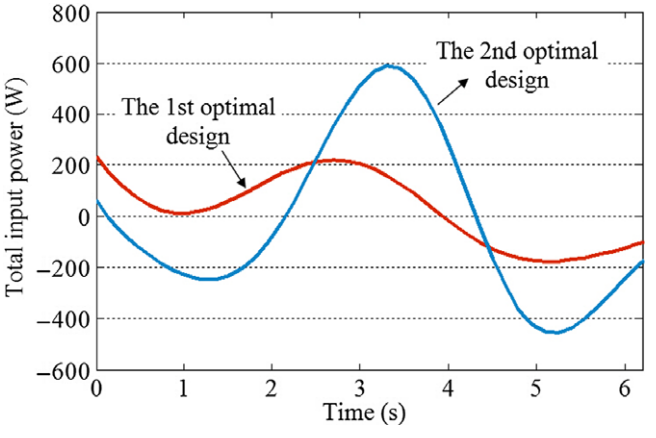

Figure 12. *The total input power of the 4RPSP+PS PM for the two selected optimal designs obtained by MOGEO.*

https://doi.org/10.1017/S0263574721000746 Published online by Cambridge University Press

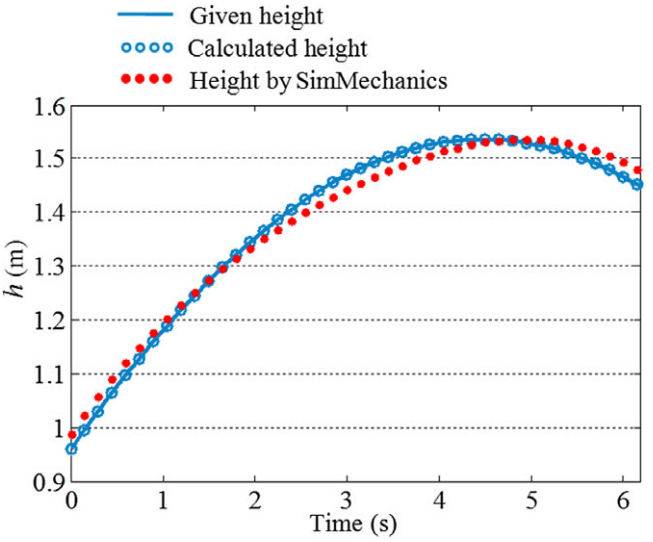

Figure 13. *The given, calculated and simulated heights of the moving platform by mathematical and SimMechanics models.*

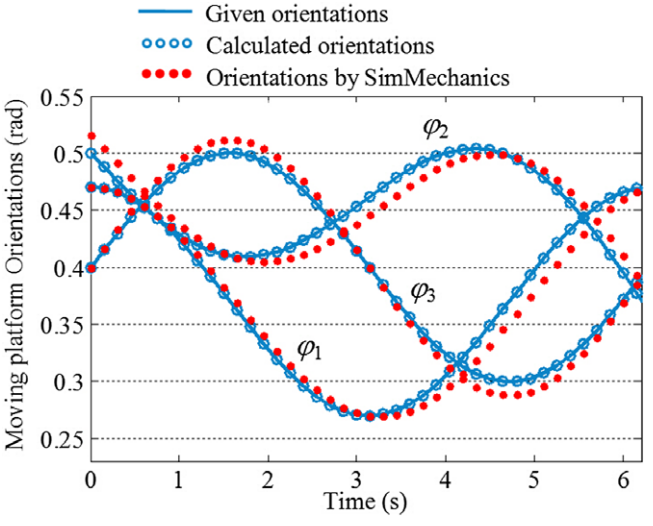

Figure 14. *The given, calculated and simulated orientations of the moving platform by mathematical and SimMechanics models.*

trajectories. The results of this numerical example verify correctness of the presented dynamic modeling and power optimization of the manipulator.

8. Conclusion

Dynamic modeling and power optimization of a 4RPSP+PS flight simulator PM were presented in this paper. After description of the manipulator structure, the coordinate frames and rotation matrices of its moving links were defined. The inverse position kinematics of the manipulator was reviewed. Through velocity analysis, Jacobian matrices of the manipulator and its moving links were obtained. Using the Euler–Lagrange method, a closed-form dynamic equation of the manipulator was derived in terms of time derivatives of pose vector **q** of the moving platform without resorting to acceleration analysis. This

https://doi.org/10.1017/S0263574721000746 Published online by Cambridge University Press

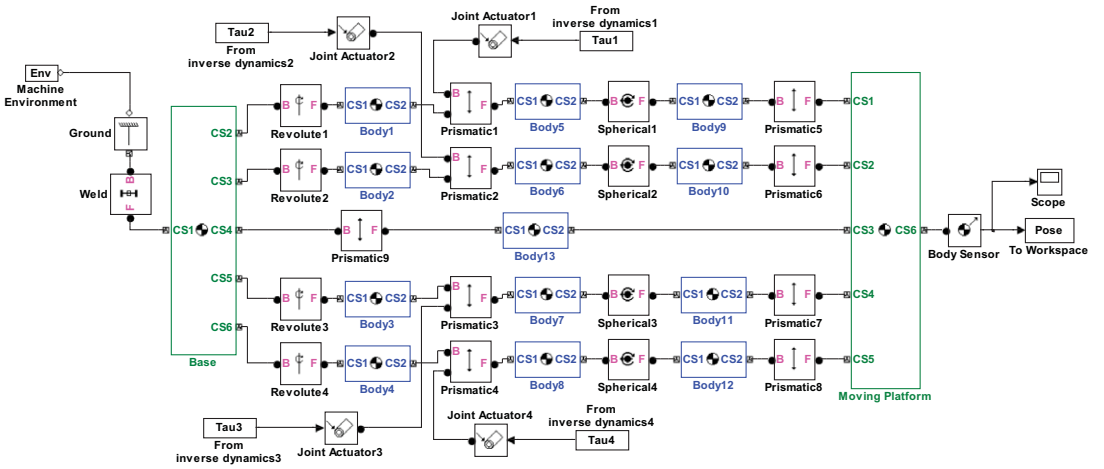

Figure 15. *SimMechanics model for forward dynamics of 4RPSP+PS PM.*

simplifies dynamic analysis of the 4RPSP+PS PM and decreases the computational time significantly. A global power transmission was defined to measure the power consumption and the energy efficiency of the manipulator in its workspace. Then, a multiobjective optimization problem was defined to maximize workspace and to minimize power consumption of the manipulator. The problem was solved by MOGEO and resulted in a Pareto front of the solutions from which a designer can easily select his/her favorite optimal design with the desired energy deficiency and workspace volume. A numerical example was presented to compare power consumptions of the two arbitrarily selected optimal designs from the Pareto front, revealing that the optimal designs with smaller workspaces have a much less power consumptions (and conversely higher energy efficiencies) than the designs with larger workspaces. In addition, dynamic modeling of the manipulator was validated by a SimMechanics model. The author hopes that the contents of this paper will be helpful for future research of the proposed 4RPSP+PS PM in the field of control and motion planning.

Conflicts of Interests The author declares no potential conflicts of interest with authorship or publication of this article.

References

[1] Wikipedia contributors, "Federal Aviation Administration," Wikipedia, The Free Encyclopedia, https://en.wikipedia.org/w/index.php?title=Federal_Aviation_Administration&oldid=986975477 (accessed November 9, 2020).

[2] D. Stewart, "A platform with six degrees of freedom," *Proc. Inst. Mech. Eng, Part A J. Power Energy* **180**(15), 371–386 (1965).

[3] Y. Song, B. Lian, T. Sun, G. Dong, Y. Qi and H. Gao, "A novel five-degree-of-freedom parallel manipulator and its kinematic optimization," *J. Mech. Rob.* **6**, 041008-1-9 (2014).

[4] Y. Zhao, K. Qiu, Sh. Wang and Z. Zhang, "Inverse kinematics and rigid-body dynamics for a three rotational degrees of freedom parallel manipulator," *Rob. Comput. Integr. Manuf.*" **31**, 40–50 (2015). doi: 10.1016/j.rcim.2014.07.002

[5] Y. Jiang, T.-m. Li and L.-p. Wang, "Dynamic modeling and redundant force optimization of a 2-DOF parallel kinematic machine with kinematic redundancy," *Rob. Comput. Integr. Manuf.* **32**, 1–10 (2015). doi: 10.1016/j.rcim.2014.08.001

[6] B. Danaei, A. Arian, M. Tale Masouleh and A. Kalhor, "Dynamic modeling and base inertial parameters determination of a 2-DOF spherical parallel mechanism," *Multibody Syst. Dyn.* **41**, 367–390 (2017). doi: 10.1007/s11044-017-9578-3

[7] S. Zarkandi, "Kinematic and dynamic modeling of a planar parallel manipulator served as CNC tool holder," *Int. J. Dyn. Control* **6**(1), 14–28 (2018).

[8] S. Zarkandi, "Kinematics, workspace and optimal design of a novel 4RSS + PS parallel manipulator," *J. Braz. Soc. Mech. Sci. Eng.* **41**, 474 (2019). doi: 10.1007/s40430-019-1981-7

[9] Y. Li, J. Wang, X.-J. Liu and L.-P. Wang, "Dynamic performance comparison and counterweight optimization of two 3-DOF parallel manipulators for a new hybrid machine tool," *Mech. Mach. Theory* **45**(11), 1668–1680 (2010). doi: 10.1016/j.mechmachtheory.2010.06.009

https://doi.org/10.1017/S0263574721000746 Published online by Cambridge University Press

[10] S. Liu, T. Huang, J. Mei, X. Zhao, P. Wang and D. G. Chetwynd, "Optimal design of a 4-DOF SCARA type parallel robot using dynamic performance indices and angular constraints," *J. Mech. Rob.* **4**(3), 031005 (2012). doi: 10.1115/1.4006743
[11] P.-L. Yen and C.-Ch. Lai, "Dynamic modeling and control of a 3-DOF Cartesian parallel manipulator," *Mechatronics* **19**(3), 390–398 (2009). doi: 10.1016/j.mechatronics.2008.09.007
[12] J. Wu, J. Wang, L. Wang and T. Li, "Dynamics and control of a planar 3-DOF parallel manipulator with actuation redundancy," *Mech. Mach. Theory* **44**(4), 835–849 (2009). doi: 10.1016/j.mechmachtheory.2008.04.002
[13] J. Yaoa, W. Gua, Z. Fenga, L. Chena, Y. Xua and Y. Zhaoa, "Dynamic analysis and driving force optimization of a 5-DOF parallel manipulator with redundant actuation," *Rob. Comput. Integr. Manuf.* **48**, 51–58 (2017). doi: 10.1016/j.rcim.2017.02.006
[14] W. Khalil and S. Guegan, "Inverse and direct dynamic modeling of Gough–Stewart manipulators," *IEEE Trans. Rob.* **20**(4), 754–761 (2004).
[15] B. Dasgupta and T. S. Mruthyunjaya, "A Newton-Euler formulation for the inverse dynamics of the Stewart platform manipulator," *Mech. Mach. Theory* **33**(8), 1135–1152 (1998).
[16] H. B. Guo and H. R. Li, "Dynamic analysis and simulation of a six degree of freedom Stewart platform manipulator," *Proc. IMechE Vol. 220 Part C: J. Mech. Eng. Sci.* **220**(1), 61–72 (2006).
[17] O. Altuzarra, A. Zubizarreta, I. Cabanes and Ch. Pinto, "Dynamics of a four degrees-of-freedom parallel manipulator with parallelogram joints," *Mechatronics* **19**(8), 1269–1279 (2009).
[18] A. Akbarzadeh and J. Enferadi, "Improved general solution for the dynamic modeling of Gough–Stewart platform based on principle of virtual work," *J. Intell. Rob. Syst.* **63**, 25–49 (2011). doi: 10.1007/s11071-015-2489-z
[19] M.-J. Liu, C.-X. Li and C.-N. Li, "Dynamics analysis of the Gough–Stewart platform manipulator," *IEEE Trans. Rob. Autom.* **16**(1), 94–98 (2000).
[20] J. Gallardo, J. M. Rico and A. Frisoli, "Dynamics of parallel manipulators by means of screw theory," *Mech. Mach. Theory* **38**(11), 1113–1131 (2003).
[21] A. Akbarzadeh, J. Enferadi and M. Sharifnia, "Dynamics analysis of a 3-RRP spherical parallel manipulator using the natural orthogonal complement," **29**(4), 361–380 (2013).
[22] K. Sugimoto, "Kinematics and dynamic analysis of parallel manipulator by means of motor algebra," *ASME J. Mech. Transm. Autom. Des.* **109**(1), 3–7 (1987).
[23] G. Carabin, E. Wehrle and R. Vidoni, "A review on energy-saving optimization methods for robotic and automatic systems," *Robotics* **6**(39), 1–21 (2017).
[24] Y. Li and G. M. Bone, Are Parallel Manipulators More Energy Efficient? *Proceedings of the 2001 IEEE International Symposium on Computational Intelligence in Robotics and Automation (Cat. No. 01EX515)*, Banff, AB, Canada (2001) pp. 41–46.
[25] Y. J. Kim, "Design of Low Inertia Manipulator with High Stiffness and Strength using Tension Amplifying Mechanisms," *Proceedings of the IEEE/RSJ International Conference on Intelligent Manipulators and Systems (IROS)*, Hamburg, Germany (2015) pp. 5850–5856.
[26] H. Yin, J. Liu and F. Yang, "Hybrid structure design of lightweight robotic arms based on carbon fiber reinforced plastic and aluminum alloy," *IEEE Access* **7**, 64932–64945(2019). doi: 10.1109/ACCESS.2019.2915363
[27] Y. He, J. Mei, J. Zang, S. Xie and F. Zhang, "Multicriteria optimization design for end effector mounting bracket of a high speed and heavy load palletizing robot," *Math. Problems Eng.* **2018**, Article ID 6049635, 17 p (2018). doi: 10.1155/2018/6049635
[28] G. Carabin, I. Palomba, E. Wehrle and R. Vidoni, "Energy Expenditure Minimization for a Delta-2 Robot Through a Mixed Approach," *Proceedings of the IFToMMWorld Congress on Mechanism and Machine Science*, Krakow, Poland (2019) pp. 383–390.
[29] P. Khalaf and H. Richter, "Trajectory optimization of manipulators with regenerative drive systems: Numerical and experimental results," *IEEE Trans. Robot* **36**(2), 501–516 (2019).
[30] P. Boscariol and D. Richiedei, "Energy-efficient design of multipoint trajectories for Cartesian manipulators," *Int. J. Adv. Manuf. Technol.* **102**, 1853–1870 (2019). doi: 10.1007/s00170-018-03234-4
[31] P. M. Ho, N. Uchiyama, S. Sano, Y. Honda, A. Kato and T. Yonezawa, "Simple motion trajectory generation for energy saving of industrial machines," *SICE J. Control Meas. Syst. Integr.* **7**, 29–34 (2014). doi: 10.1109/SII.2012.6427362
[32] G. Carabin, R. Vidoni and E. Wehrle, "Energy Saving in Mechatronic Systems Through Optimal Point-to-Point Trajectory Generation Via Standard Primitives," *Proceedings of the International Conference of IFToMM ITALY*, Cassino, Italy, 29–30 (2018) pp. 20–28.
[33] G. Lee, S. Park, D. Lee, F. C. Park, J. I. Jeong and J. Kim, "Minimizing energy consumption of parallel mechanisms via redundant actuation," *IEEE/ASME Trans. Mech.* **20**(6), 2805–2812 (2015). doi: 10.1109/TMECH.2015.2401606
[34] G. Lee, S. K. Sul and J. Kim, "Energy-saving method of parallel mechanism by redundant actuation," *Int. J. Precis. Eng. Manuf. Green Tech.* **2**, 345–351 (2015). doi: 10.1007/s40684-015-0042-7
[35] A. Gómez Ruiz, J. Cavalcanti Santos, J. Croes and W. Desmet, "On redundancy resolution and energy consumption of kinematically redundant planar parallel manipulators," *Robotica* **36**(6), 809–821 (2018).
[36] P. Boscariol and D. Richiedei, "Trajectory design for energy savings in redundant robotic cells," *Robotics* **8**(1), 15 (2019). doi: 10.3390/robotics8010015

https://doi.org/10.1017/S0263574721000746 Published online by Cambridge University Press

[37] P. Boscariol, L. Scalera and A. Gasparetto, "Task-Dependent Energetic Analysis of a 3 DOF Industrial Manipulator," *Proceedings of the International Conference on Robotics in Alpe-Adria Danube Region*, Kaiserslautern, Germany, 19–21 (2019) pp. 162–169.
[38] L. Scalera, P. Boscariol, G. Carabin, R. Vidoni and A. Gasparetto, "Enhancing energy efficiency of a 4-DOF parallel robot through task-related analysis," *Machines* **8**(1), 10 (2020). doi: 10.3390/machines8010010
[39] R. Boudreau, J. Léger, H. Tinaou and A. Gallant, "Dynamic analysis and optimization of a kinematically redundant planar parallel manipulator," *Trans. Canad. Soc. Mech. Eng*. **42**(1), 20–29 (2018). doi: 10.1139/tcsme-2017-0003
[40] S. Park, J. Kim and G. Lee, "Optimal trajectory planning considering optimal torque distribution of redundantly actuated parallel mechanism," *Proc. Inst. Mech. Eng. Part C J. Mech. Eng. Sci.* **232**(23), 4410–4419 (2018). doi: 10.1177/0954406217751818
[41] J. P. Barreto and B. Corves, "Matching the Free-Vibration Response of a Delta Robot with Pick-and-Place Tasks Using Multi-Body Simulation," *2018 IEEE 14th International Conference on Automation Science and Engineering (CASE)*, Munich, Germany (2018) pp. 1487–1492. doi: 10.1109/COASE.2018.8560393
[42] L. Scalera, G. Carabin, R. Vidoni and T. Wongratanaphisan, "Energy efficiency in a 4-DOF parallel robot featuring compliant elements," *Int. J. Mech. Control* **20**(02), 49–57 (2019).
[43] X. Liu, W. Bi and F. Xie, "An energy efficiency evaluation method for parallel manipulators based on the kinetic energy change rate," *Sci. China Technol. Sci.* **62**, 1035–1044 (2019). doi: 10.1007/s11431-019-9487-7
[44] S. Zarkandi, "Kinematic analysis and workspace optimization of a novel 4RPSP + PS parallel manipulator," *Mech. Based Des. Struct. Mach.* (2020). doi: 10.1080/15397734.2020.1725564
[45] L.-W. Tsai, *Robot Analysis and Design: The Mechanics of Serial and Parallel Manipulators, Section 9.8* (John Wiley & Sons, Inc., 1999). ISBN:0471325937.
[46] H. Goldstein, *Classical Mechanics*, 2nd ed. (Addison-Wesley, Reading, MA, 1980).
[47] A. Mohammadi-Balani, M. Dehghan Nayeri, A. Azar and M. Taghizadeh-Yazdi, "Golden eagle optimizer: A nature-inspired metaheuristic algorithm," *Comput. Ind. Eng.* **152** (2021). doi: 10.1016/j.cie.2020.107050
[48] C. A. Coello Coello and M. S. Lechuga, "MOPSO: A Proposal for Multiple Objective Particle Swarm Optimization," *Proceedings of the 2002 Congress on Evolutionary Computation. CEC'02 (Cat. No.02TH8600),* Honolulu, HI, USA, vol. 2 (2002) pp. 1051–1056. doi: 10.1109/CEC.2002.1004388

Appendix A

Values of architecture parameters:

$$a = 0.5m, l_{pl} = 1.5m, l_{cyl} = 0.55m, l_{pis} = 0.5m$$

Mass properties of the simulator machine:

$$m_{pl} = 1.5kg, m_{mp} = 3.5kg, m_{sc} = 14kg, \mathbf{d}_{sc} = [001.1]^T m,$$

$$\bar{\mathbf{I}}_{mp} = \begin{bmatrix} 1.82 & 0 & 0 \\ 0 & 1.82 & 0 \\ 0 & 0 & 1.65 \end{bmatrix} kg.m^2, \bar{\mathbf{I}}_{sc} = \begin{bmatrix} 10.82 & 0 & 0 \\ 0 & 7.33 & 0 \\ 0 & 0 & 8.54 \end{bmatrix} kg.m^2$$

$$m_{cyl} = 1.75kg, kg, \bar{\mathbf{I}}_{cyl} = \begin{bmatrix} 0.89 & 0 & 0 \\ 0 & 0.89 & 0 \\ 0 & 0 & 0.24 \end{bmatrix} kg.m^2$$

$$m_{pis} = 1.65kg, \bar{\mathbf{I}}_{pis} = \begin{bmatrix} 0.79 & 0 & 0 \\ 0 & 0.79 & 0 \\ 0 & 0 & 0.33 \end{bmatrix} kg.m^2$$

$$m_{bl} = 0.25kg, \bar{\mathbf{I}}_{bl} = \begin{bmatrix} 0.33 & 0 & 0 \\ 0 & 0.23 & 0 \\ 0 & 0 & 0.27 \end{bmatrix} kg.m^2$$

Cite this article: S. Zarkandi (2022). "Dynamic modeling and power optimization of a 4RPSP+PS parallel flight simulator machine", Robotica **40**, 646–671. https://doi.org/10.1017/S0263574721000746

https://doi.org/10.1017/S0263574721000746 Published online by Cambridge University Press